ORIGINAL RESEARCH

Aryl Hydrocarbon Receptor Nuclear Translocator in Vascular Smooth Muscle Cells Is Required for Optimal Peripheral Perfusion Recovery

Anna Henry Borton, BChE; Bryan L. Benson, BS; Lee E. Neilson, MD; Ashley Saunders, BS; M. Amer Alaiti, MD; Alex Y. Huang, MD, PhD; Mukesh K. Jain, MD; Aaron Proweller, MD, PhD; Diana L. Ramirez-Bergeron, PhD

***Background*—**Limb ischemia resulting from peripheral vascular disease is a common cause of morbidity. Vessel occlusion limits blood flow, creating a hypoxic environment that damages distal tissue, requiring therapeutic revascularization. Hypoxia-inducible factors (HIFs) are key transcriptional regulators of hypoxic vascular responses, including angiogenesis and arteriogenesis. Despite vascular smooth muscle cells' (VSMCs') importance in vessel integrity, little is known about their functional responses to hypoxia in peripheral vascular disease. This study investigated the role of VSMC HIF in mediating peripheral ischemic responses.

***Methods and Results*—**We used $Arnt^{SMKO}$ mice with smooth muscle–specific deletion of aryl hydrocarbon receptor nuclear translocator (ARNT, HIF-1β), required for HIF transcriptional activity, in a femoral artery ligation model of peripheral vascular disease. $Arnt^{SMKO}$ mice exhibit impaired perfusion recovery despite normal collateral vessel dilation and angiogenic capillary responses. Decreased blood flow manifests in extensive tissue damage and hypoxia in ligated limbs of $Arnt^{SMKO}$ mice. Furthermore, loss of aryl hydrocarbon receptor nuclear translocator changes the proliferation, migration, and transcriptional profile of cultured VSMCs. $Arnt^{SMKO}$ mice display disrupted VSMC morphologic features and wrapping around arterioles and increased vascular permeability linked to decreased local blood flow.

***Conclusions*—**Our data demonstrate that traditional vascular remodeling responses are insufficient to provide robust peripheral tissue reperfusion in $Arnt^{SMKO}$ mice. In all, this study highlights HIF responses to hypoxia in arteriole VSMCs critical for the phenotypic and functional stability of vessels that aid in the recovery of blood flow in ischemic peripheral tissues. **(*J Am Heart Assoc*. 2018;7:e009205. DOI: 10.1161/JAHA.118.009205.)**

Key Words: aryl hydrocarbon receptor nuclear translocator • hind-limb ischemia • hypoxia • peripheral vascular disease • vascular biology • vascular smooth muscle • Hypoxia-inducible Factor

Limb ischemia is a sequela of peripheral vascular disease, a major cause of morbidity affecting millions of people worldwide.[1] Arterial occlusion limits blood flow, creating a hypoxic environment and damaging tissue, which in severe cases can necessitate amputation. Vascular responses to episodes of ischemia attempt to restore perfusion through arteriogenic processes of redirecting blood flow through extant collateral circulation and angiogenic processes initiating de novo growth of vessels to regenerate the downstream vascular network.[2–4] Although the role of endothelial cells (ECs) in initiating and effectuating these responses has been extensively examined, far less is known about the contributions and regulators of neighboring vascular smooth muscle cells (VSMCs).

In response to various physiological stresses, VSMCs undergo phenotypic switching, permitting them to proliferate and migrate, contributing to the remodeling of the vascular wall in pulmonary hypertension, systemic hypertension, and

From the Department of Pathology (A.H.B., B.L.B., A.Y.H.), Case Cardiovascular Research Institute (A.H.B., A.S., M.A.A., M.K.J., A.P., D.L.R.-B.), Division of Pediatric Hematology-Oncology, Department of Pediatrics (A.Y.H.), and Case Comprehensive Cancer Center (A.Y.H.), Case Western Reserve University School of Medicine, Cleveland, OH; and Harrington Heart and Vascular Institute (A.H.B., A.S., M.A.A., M.K.J., A.P., D.L.R.-B.), Neurological Institute (L.E.N.), and Angie Fowler Adolescent and Young Adult Cancer Institute and University Hospitals Rainbow Babies and Children's Hospital (A.Y.H.), University Hospitals, Cleveland, OH.

Accompanying Table S1 and Figures S1 through S5 are available at http://jaha.ahajournals.org/content/7/11/e009205/DC1/embed/inline-supplementary-material-1.pdf

Correspondence to: Diana L. Ramirez-Bergeron, PhD, Case Western Reserve University School of Medicine, 2103 Cornell Rd, Cleveland, OH 44106. E-mail: dlr36@case.edu

Received March 20, 2018; accepted May 2, 2018.

Clinical Perspective

What Is New?

- Vascular smooth muscle cell (VSMC)–specific disruption of hypoxia-inducible factor, through deletion of aryl hydrocarbon receptor nuclear translocator (hypoxia-inducible factor-1β subunit), impairs reperfusion after femoral artery ligation.
- Ligated limbs of VSMC aryl hydrocarbon receptor nuclear translocator knockout mice show increased tissue damage, hypoxia, and vascular permeability despite dynamic signs of arteriogenesis and angiogenesis.
- Loss of aryl hydrocarbon receptor nuclear translocator disrupts arteriolar VSMC morphologic features.
- Hypoxia's capacity to regulate the molecular markers of VSMC structure, homeostasis, proliferation, and migration is aryl hydrocarbon receptor nuclear translocator dependent.

What Are the Clinical Implications?

- Hypoxia-inducible factor–driven responses of VSMCs are essential for full recovery in peripheral ischemia; thus, VSMCs are important targets to consider for therapeutic interventions.

atherosclerosis, among others.[5,6] For many of these conditions, hypoxia is an important pathologic trigger. Hypoxia-inducible factors (HIFs) are heterodimeric transcription factors, composed of HIF-α and aryl hydrocarbon receptor nuclear translocator (ARNT; HIF-β) subunits, essential for cellular responses to hypoxia.[7–13] In the presence of O_2, HIF-1α and HIF-2α are hydroxylated and targeted for proteasomal degradation. Hypoxic conditions inhibit the hydroxylation of α-subunits, which dimerize with ubiquitously expressed ARNT to form active HIF-1 or HIF-2 functioning as master regulators of O_2 homeostasis by binding to and activating gene promoters containing hypoxia response elements.[12] Although HIF-2's expression and activity are more restricted, HIF-1 has been implicated in the transcriptional regulation of hundreds of genes, including many involved in vascular growth and remodeling.[14–16]

Hypoxia and HIFs have been studied extensively in VSMCs of the pulmonary vasculature. In the context of hypoxia-driven pulmonary hypertension, HIF-1 is essential for VSMC proliferation in vivo.[17–19] However, the pulmonary vasculature differs from the systemic vasculature in hemodynamic forces and O_2 status, suggesting that these results may not be directly translatable to other arterial beds. Studies of the role of HIF in VSMCs outside of the pulmonary circulation are limited and have primarily focused on examining the interplay between HIF-1 and angiotensin II signaling in vascular remodeling of the aorta.[20,21]

A considerable body of literature demonstrates the involvement of HIF in response to peripheral ischemia. Human patients with critical limb ischemia exhibit changes in HIF-1α protein levels and vascular density.[22] Increased levels of stabilized HIF-1α are also seen in mouse models of hind-limb ischemia (HLI) induced by femoral artery ligation.[23] Although global *Hif-1α*$^{+/-}$ mice show decreased blood reperfusion after ligation, injection of stabilized HIF-1α in ischemic muscle promotes angiogenesis and arteriogenesis, thereby increasing reperfusion.[23–26] Specific to vascular cells, EC responses are known to be dependent on HIFs, with EC-specific knockouts of HIF-2α displaying decreased blood flow after induction of HLI attributable to aberrant arteriogenic and angiogenic responses.[27] Most recently, VSMC HIF-1α knockout mice were characterized with decreased limb reperfusion after femoral artery ligation attributable to the enhanced production of thrombospondin-2, known to inhibit angiogenesis.[28] However, although HIFs' regenerative vascular properties have been well described in the nontargeted and EC contexts, the specific mechanisms of revascularization dependent on HIF-driven VSMC responses to peripheral ischemia are not well described.

The following studies tested the hypothesis that endogenous HIF in VSMCs contributes to peripheral perfusion recovery. Canonical HIF transcriptional activity was ablated in VSMCs in vivo through the tissue-specific deletion of ARNT, the required HIF-β subunit. Our findings reveal impaired reperfusion after femoral artery ligation despite signs of arteriogenesis and angiogenesis. Evidence of disrupted VSMC organization at the arteriolar level implicate VSMCs as central to this deficit. Moreover, this study finds hypoxia's capacity to regulate the molecular markers of VSMC structure, homeostasis, proliferation, and migration is ARNT dependent. Our findings underscore the essential role of HIF-dependent hypoxia-driven responses by VSMCs to achieve optimal peripheral perfusion recovery.

Methods

The data, analytic methods, and study materials will be made available on reasonable request to other researchers for purposes of reproducing the results or replicating the procedure.

Mouse Generation

Previously described *SM22α-Cre*$^{+/-}$ and *Arnt*$^{lox/lox}$ mice were crossed and maintained in a C57Bl/6j background.[29–33] The progeny of *SM22α-Cre*$^{+/-}$ *Arnt*$^{+/lox}$×*Arnt*$^{lox/lox}$ were used for experiments. *Arnt* deletion was verified by protein and mRNA levels in aortic VSMCs isolated and cultured, as described later. Sex- and litter-matched, or if unavailable, aged-matched *Cre*$^{-}$ *Arnt*$^{lox/lox}$ or *Cre*$^{-}$ *Arnt*$^{wt/lox}$ mice were selected as controls. All animal studies were performed with the approval

of the Case Western Reserve University Institutional Animal Care and Use Committee.

Echocardiography

For transthoracic echocardiography, mice were anesthetized by inhalation of 1% isoflurane with O_2. All data were recorded and analyzed by the VEVO 770 High Resolution Imaging System (Fujifilm Visual Sonics Inc) and the RMV-707B 30-MHz probe. In M-mode short-axis images, ejection fraction and fractional shortening were measured at the papillary muscle level. Measurements were acquired at heart rates >500 beats per minute.

HLI Model

HLI procedure, tissue harvest for frozen preparation, and pigment perfusion were performed as previously described, with minor modifications.[34] Briefly, 8- to 12-week-old mice, assigned a number for blinding purposes, were anesthetized by IP injection of ketamine (80 mg/kg) and xylazine (7 mg/kg). Surgical depth of anesthesia was verified by toe pinch. After hair removal, preoperative perfusion assessment, and preparation of the surgical field, an incision was made in the left inner thigh. Blunt dissection was used to visualize and separate the femoral artery from the neighboring vein and nerve. Two ligatures of 7-0 braided silk suture were placed on the superficial femoral artery distal to the branching of the deep femoral artery and proximal to the popliteal bifurcation, and the intervening artery was cut. Alternatively, a more severe model of HLI was achieved by placing both ligatures proximal to the branching of the deep femoral artery. The epigastric artery was dissected and cauterized (Bovie). Wound clips (7.5 mm; Michel) and 6-0 polypropylene suture were used to close the incision. Postoperative analgesia with buprenorphine (0.06 mg/kg; IP; every 12 hours) was administered for 3 days. Male mice were used for these studies because of previously described improved HLI recovery in male versus female mice,[35] allowing more dynamic range and increasing power to detect recovery deficits.

To assess perfusion, mice were anesthetized, as previously described, and placed on 37°C heating pad for 5 minutes before scanning. Infrared laser Doppler scans of the foot pad were performed at 4 ms/pixel in triplicate on a MOORLDI2-IR (Moore Instruments Ltd). Mean blood flow on flux images was assessed by moorLDI v5.0 software package. Perfusion heat maps for visual display are presented with palate limits of 0 and 2000.

Where indicated, 594-conjugated lycopersicon esculentum lectin (100 μL; DL-1177; Dylight) was administered via the jugular vein and allowed to circulate for 5 minutes at 7 days after HLI. For vascular permeability assessments, 2 mg of 2000-kDa fluorescein isothiocyanate (FITC)–dextran (FD2000S; Sigma) was administered via tail vein, 2 hours before euthanasia. In anesthetized mice, the chest was opened and the left ventricle was cannulated and infused with vasodilation solution (10 U/mL heparin [Sigma], 100 μmol/L adenosine [Sigma], 100 μmol/L papaverine hydrochloride [Sigma], 0.05% wt/vol BSA [fraction V; Fisher] in Ca^+ Mg^+ Dulbecco's PBS [Invitrogen]) at 10 mL/min, followed by warm 10% neutral-buffered formalin or pigmented fixation solution (8 g gouache [470; Winsor & Newton] in 50 mL 4% paraformaldehyde). Some mice were injected IP with the hypoxic marker pimonidazole {1-[(2-hydroxy-3-piperidinyl)propyl]-2-nitroimidazole} hydrochloride (60 mg/kg; Hypoxyprobe, Inc) 30 minutes before euthanasia to visualize hypoxic regions.

Collateral Assessment

Limbs perfused with pigmented fixation solution were removed at the hip. After removing the skin, limbs were dehydrated to 100% methanol and the tissues were cleared with 1:1 benzyl alcohol/benzyl benzoate. Vessels were imaged with Leica MZ 16 FA at ×10, without a filter, and ×65, with a green fluorescent protein filter for improved contrast. Average diameter was quantified in ImageJ as the dividend of the vessel profile area and the vessel length from tiled ×65 images segmented in Photoshop (Adobe).

Histological and Immunohistochemistry Features

Gastrocnemius muscles for histological assessment were harvested, cryoprotected in 15% sucrose, then 30% sucrose overnight, embedded in optimal cutting temperature compound (Tissue Tek), frozen, and stored at −80°C. Serial transverse sections (8-μm thick) of gastrocnemius muscle were obtained with a cryostat (Leica CM 1850 UV) and postfixed in 2% paraformaldehyde. For damage assessment, sections were stained with hematoxylin and eosin and imaged with Leica DM 2000LED (×40 objective). For capillary quantification, sections were blocked with 2% BSA and 5% normal goat serum in PBS and subsequently incubated with anti-CD31 (1:50; 550274; BD-Pharmingen), followed by goat anti-rat IgG-488 (1:200; A-11006; Invitrogen) and, where indicated, Cy3-conjugated α-smooth muscle actin (SMA; 1:400; C6198; Sigma). To detect areas of hypoxia, 0.1% Triton X-100 was added to the blocking buffer above, followed by FITC-conjugated mouse anti-pimonidazole (1:200; Hypoxyprobe). Tissues were counterstained with 4′,6-diamidino-2-phenylindole in mounting medium (Vector). Images were captured on a Leica DMI 6000 B with a ×10 objective. For myocyte enumeration, gastrocnemius sections were labeled with 5 μg/mL wheat germ agglutinin, Oregon green-488 (W7024; Invitrogen) in PBS. Damaged and hypoxic areas were quantified as a percentage of gastrocnemius cross-sectional area in ImageJ. $CD31^+$ capillaries, $lectin^+$ vessels, SMA^+ VSMCs, and skeletal myocytes were enumerated in blinded raw images

collected at the same exposure. For each limb, 6 301-μm^2 regions of 2 gastrocnemius sections were quantified.

Arteriole Imaging in Spinotrapezius Whole Mount

Collection and visualization of vessels in the spinotrapezius has been previously described.[36] Briefly, after euthanasia with CO_2 and left ventricular infusion of warm PBS, spinotrapezius muscles were collected and fixed in 4% paraformaldehyde in PBS for 20 minutes at room temperature. Tissues were blocked with 2% BSA and 0.3% Triton X-100 in PBS overnight at 4°C. VSMCs were identified by FITC-conjugated anti-SMA (1:400; F3777; Sigma). Confocal images were taken on a Leica SP5 DMI 6000B using argon 488-nm and helium-neon 633-nm laser lines with a Leica 506192 HCX PL APO λ blue ×63/1.4 oil objective with 0.17-mm glass correction. For detection, 12-bit photomultiplier tubes were used with Leica LAS AF acquisition software.

Vascular Imaging in Thick Sections of Gastrocnemius Muscles

After post-HLI tissue collection, as previously described, 400-μm coronal sections of gastrocnemius muscle were cut by vibratome (Leica VT 1200). Sections were blocked with 5% normal goat serum, 2% BSA, and 0.3% Triton X-100 in PBS. In permeability studies, vessels were labeled with anti-CD31 (1:50; 550274; BD-Pharmingen), followed by goat anti-rat IgG-647 (1:200; A21247; Invitrogen). VSMCs were labeled with FITC-conjugated anti-SMA (1:400; F3777; Sigma). A Leica SP5 confocal microscope equipped with a ×20 water immersion lens (Leica HCX-APO-L; numerical aperture, 1.0) and a tunable 16W Ti/Sapphire IR laser tuned to 800 nm (Chameleon Coherent, Inc) was used for 2-photon laser scanning microscopy imaging using nondescanned detectors set to capture Alexa Fluor 647 CD31 and/or FITC (dextran or SMA) fluorescence. For perfusion imaging, XYZ images with an XY dimension of 775×775 μm were obtained at 512×512 pixels in 5-μm z stacks. For SMA imaging of gastrocnemius muscle, XYZ images with an XY dimension of 310×310 μm were obtained at 1024×1024 pixels in 1.95-μm z stacks.

Confocal and Multiphoton Image Processing

High-resolution confocal and multiphoton images were deconvolved by Huygens Professional 16.10 using classic maximum likelihood estimation at an estimated signal/noise ratio of 5. Point spread functions were estimated a priori in Huygens Professional using the wavelengths of excitation and emission light, position of the cover slip and orientation of the lens, lens immersion and specimen mounting media, and pinhole radius. These parameters were held identical within sets of images. After restoration, data were imported to Imaris (BitPlane, Inc) to generate figures. Low-resolution confocal images were not deconvolved, and a median filter of 3×3 voxels was applied in Imaris. Because of inhomogeneities in SMA staining intensity between and within tissues, brightness and contrast were adjusted to facilitate comparison of smooth muscle cell architecture.

Cell Culture

Isolation and culture of primary aortic VSMCs were performed as previously described.[30] Briefly, explants of thoracic aorta were divided longitudinally and plated lumen side down in 1-mm^2 pieces on 2 tissue culture dishes and covered with glass cover slips. Plates were incubated in DMEM/F12 supplemented with GlutaMAX-1 (10565-018; Gibco) and 20% fetal bovine serum (FBS; Atlanta or Gemini bioproducts). After 2 weeks of growth at 37°C and 5% CO_2, explants and cover slips were removed, and media was reduced to 10% FBS. For transcription analysis, the following day, cells were starved in DMEM/F12+0.5% FBS for 16 hours, then exposed to 2% O_2 (hypoxia) or 21% O_2 (normoxia) for 24 hours in DMEM/F12+10% FBS.

Proliferation assays

VSMC cultures (20 000 cells per well) were plated in 12-well plates. After 16 hours of starvation in serum-free DMEM/F12, cells were exposed to hypoxia or normoxia in DMEM/F12+5% FBS. At 24 hours of exposure, 5-bromo-2′-deoxyuridine was added to 10 μmol/L and incubated for an additional 8 hours in normoxia or hypoxia. Cells were fixed in 4% paraformaldehyde, followed by antigen retrieval with 1 mol/L HCl, and blocking with 0.75% BSA and 0.1% Triton X-100. 5-Bromo-2′-deoxyuridine–positive cells were labeled with anti–5-bromo-2′-deoxyuridine (1.25 μg/mL; B44; BD Biosciences) and counterstained with 4′,6-diamidino-2-phenylindole (H-1200; Vectashield). Assays were performed in triplicate. Six representative images from each well were quantified.

Migration assay

Cells were plated at confluence and starved for 16 hours in serum-free DMEM/F12. After scratch with 200-μL standard pipette tip, cultures were placed in normoxia or hypoxia in DMEM/F12+0.5% FBS+25 ng/mL platelet-derived growth factor (PDGF)-BB (315-18; PeproTech). Migration distance was quantified from phase-contrast images taken at 0 and 6.5 hours and analyzed using NIH ImageJ software.

Real-Time Reverse Transcription–Polymerase Chain Reaction

Total RNA was isolated from cultured cells using TRIzol reagent (Ambion). RNA was reversed transcribed to cDNA with QuantiTect reverse transcription kit (205311; Qiagen).

Relative expression was quantified in technical triplicates by real-time quantitative reverse transcription–polymerase chain reaction using the FastStart Universal SYBR Green Master (ROX) Mix (04913850001; Roche) on a StepOnePlus system (Applied Biosystems). Target gene expression was analyzed using the $2^{-\Delta\Delta Ct}$ method (threshold values) with normalization to 18S ribosomal RNA.[37] Results are reported as gene expression relative to *Arnt*$^{lox/lox}$ in normoxia. Primers used for target genes are presented in Table S1.

Western Blotting

Cell extraction buffer (FNN0011; Invitrogen) supplemented with cOmplete protease inhibitor cocktail and PhosSTOP phosphatase inhibitor cocktail (04693159001 and 04906845001, respectively; Roche) was used to collect protein from either samples of gastrocnemius muscle through bead homogenization (Qiagen TissueLyserII) or VSMCs in culture. Protein was quantified by bicinchoninic acid. Cell lysate (40 μg) or 100 μg of gastrocnemius lysate in SDS sample buffer (Boston Bioproducts) was run on 8% polyacrylamide gels in tris-glycine-SDS running buffer. Semidry transfer to nitrocellulose membrane was conducted in transfer buffer with 20% methanol. Western blots of total protein isolates were probed overnight at 4°C with rabbit anti-ARNT (1:800; 5537S; Cell Signaling) diluted in Pierce protein-free T20 (tris-buffered saline) blocking buffer (37571; Thermo Scientific). To detect the protein bands, blots were washed and probed with secondary horseradish peroxidase–linked anti-rabbit IgG (1:1000 or 1:2000; 7074S; Cell Signaling) and detected by enhanced chemiluminescence, according to the manufacturer's instructions (32106; Pierce). Membranes were stripped (21059; Thermo Scientific) and reprobed with β-actin rabbit antibody (1:5000; 4967S; Cell Signaling).

Statistical Analysis

Results are reported as the mean±SEM. Statistical analyses were performed as identified in each figure legend. Normality and homoscedasticity were evaluated with Shapiro-Wilks test and F test or Brown-Forsythe. Post testing used Tukey's multiple comparisons test for 1- and 2-way ANOVAs, Bonferroni's multiple comparisons test for repeated-measures 2-way ANOVA, and 2-stage linear step-up procedure of Benjamini, Krieger, and Yekutieli for Kruskal-Wallis test (GraphPad). Significance was defined as $P<0.05$.

Results

Generation of Smooth Muscle–Specific *Arnt* Knockout Mouse Model

To examine the role of HIF signaling in vascular smooth muscle, we generated a model of *Arnt* deletion to disrupt HIF canonical transcriptional activity and avoid compensatory changes in other HIF family members, which can confound single α-subunit deletion models.[38,39] The smooth muscle specificity of this deletion was accomplished by crossing well-characterized *SM22α-Cre* mice[29–31] with *Arnt*$^{lox/lox}$.[32] Primary aortic VSMCs isolated from *SM22α-Cre*$^{+/-}$*Arnt*$^{lox/lox}$ mice (*Arnt*^{SMKO}) show loss of *Arnt* expression at the mRNA and protein levels (Figure 1A and 1B). Maintenance of ARNT expression in skeletal muscle was assessed in bulk tissue samples of gastrocnemius muscle. Similar ARNT mRNA and protein levels were present in gastrocnemius muscles of *Arnt*^{SMKO} and *Arnt*$^{lox/lox}$ mice (Figure 1C and 1D). *Arnt*^{SMKO} mice display no overt phenotypes, with similar weight, appearance, and longevity to littermate controls (*Arnt*$^{lox/lox}$) (Figure 1E and data not shown). Because *SM22α-Cre* has demonstrated activity in cardiac tissue,[29] cardiac function was assessed by echocardiography.[40] No differences were seen in heart rate, ejection fraction, fractional shortening, or left ventricle mass of *Arnt*^{SMKO} compared with *Arnt*$^{lox/lox}$ littermate controls (Figure 1F through 1I). These results indicate that mice with tissue-specific deletion of *Arnt* in the smooth muscle appear healthy overall, without compromise of cardiac function.

Arnt^{SMKO} Mice Show Impaired Blood Flow Recovery in HLI Model

Although atherosclerotic obstruction of peripheral arteries ordinarily contributes to peripheral vascular disease in humans, we used inducible HLI, the most common mouse model of peripheral vascular disease. The superficial femoral artery was surgically ligated distal to the deep femoral artery, restricting downstream blood flow to the limb. Peripheral perfusion recovery in the foot pad was examined by infrared laser Doppler at 3, 7, 14, and 21 days after ligation (Figure 2A). Results, expressed as ratio of flow in ligated/unligated limb, show decreased perfusion recovery in the ligated limbs of *Arnt*^{SMKO} mice compared with *Arnt*$^{lox/lox}$ littermate controls beginning at day 7, with continued separation through day 21 after femoral artery ligation (Figure 2B). Recovery of blood flow in *Arnt*^{SMKO} mice is not only slower, but also plateaus at a lower level than controls. By day 7, a gap in perfusion of ≈20% emerges, closing by only an additional 5% over the subsequent 2 weeks. Functional motor recovery, evaluated using a 0- to 3-point scale from full function of foot flexion and toe grasp to dragging of the ligated limb, was delayed in *Arnt*^{SMKO} mice, although this did not achieve statistical significance (Figure 2C). Collectively, mice lacking ARNT in vascular smooth muscle demonstrate a significant and persistent disruption in perfusion recovery after femoral artery ligation.

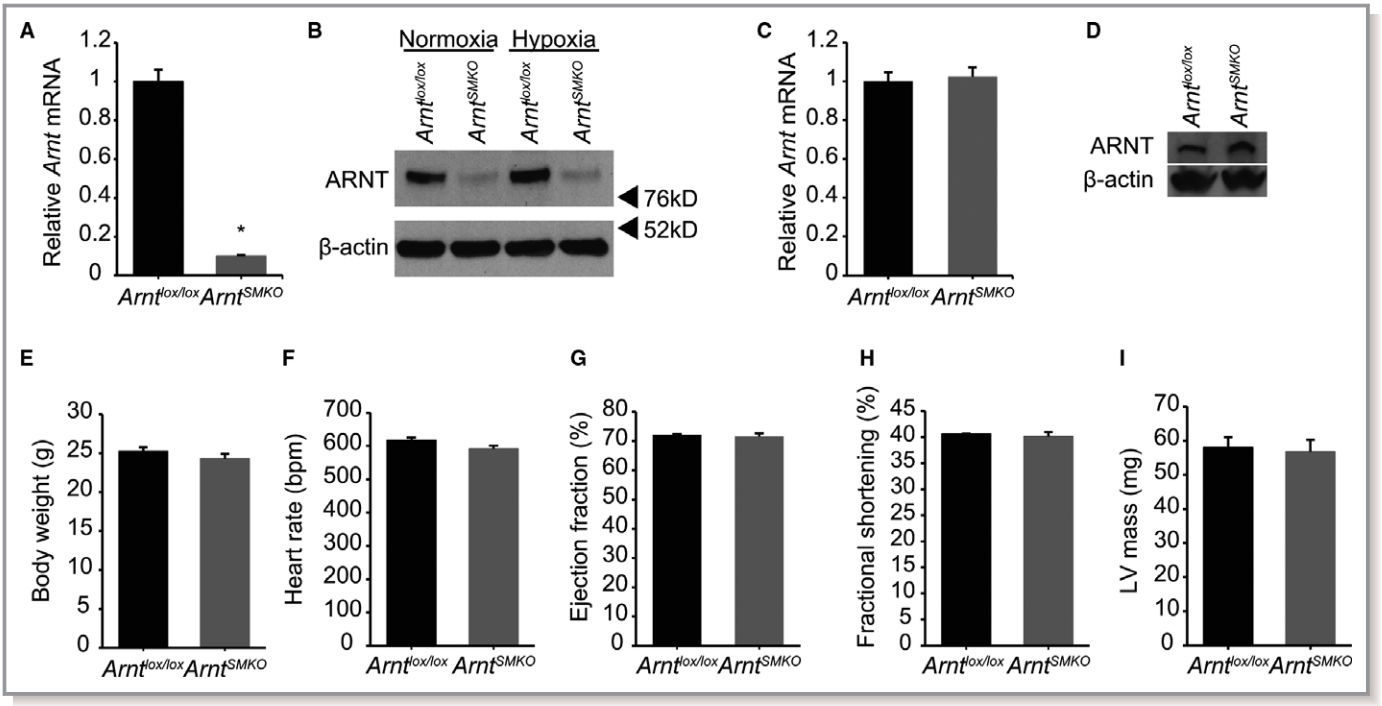

Figure 1. Characterization of *Arnt*^{SMKO} mice. Isolated aortic vascular smooth muscle cells from *Arnt*^{SMKO} mice show loss of aryl hydrocarbon receptor nuclear translocator (ARNT) expression in mRNA (n=5; A) and total protein (n=3; B). Tissue samples from gastrocnemius muscle show no differences in bulk ARNT expression in mRNA (n=5; C) or total protein (n=4; D). E, Body weights of male mice are similar in *Arnt*^{SMKO} (n=8) and *Arnt*$^{lox/lox}$ (n=11) littermates. Smooth muscle–specific ARNT deletion does not compromise cardiac function assessed by heart rate (F), ejection fraction (G), fractional shortening (H), and left ventricular (LV) mass (I) on echocardiogram (n=5). Unpaired 2-tailed *t* test (A through F, H, and I) with Mann-Whitney test (G) or Welch's correction (H) was used. *P<0.05.

Limb Ischemia Stimulates Collateral Remodeling in *Arnt*^{SMKO} and *Arnt*$^{lox/lox}$ Mice

Appearance of perfusion deficits in the first week after ligation and previously described roles for smooth muscle in arteriogenic responses prompted assessment of collateral vessel dilation and remodeling. Luminal diameters of collateral blood vessels branching proximal to the ligation and traveling through the adductor muscles were visualized by pigment perfusion and subsequent tissue clearance, which revealed similar collateral patterning and diameter in unligated limbs of *Arnt*$^{lox/lox}$ and *Arnt*^{SMKO} mice (Figure 3A through 3C). At 7 days after ligation, the time point with the largest perfusion deficit in *Arnt*^{SMKO}, we observed significant collateral vessel dilation in the ligated limbs of either mouse genotype (Figure 3A through 3C). Surprisingly, despite lower levels of distal limb perfusion, collateral vessels in *Arnt*^{SMKO} have significantly larger lumen diameters than those in control animals (Figure 3C). Flow rate through a vessel is proportional to its cross-sectional area, indicating that collaterals in *Arnt*^{SMKO} have, on average, 2.5-fold higher projected flow than the analogous vessels in *Arnt*$^{lox/lox}$ mice (Figure 3D). The collateral cross-sectional area is inversely correlated with perfusion of the limb; mice with the lowest perfusion had the largest diameter collaterals (Figure S1). These results suggest that the observed deficit perfusion in *Arnt*^{SMKO} is not attributable to inadequate collateral vessel dilation.

Early Capillary Angiogenesis Does Not Depend on VSMC *Arnt* in HLI

With sufficient collateralization observed, we next evaluated the angiogenic response to induced ischemia in the downstream vascular beds. A more severe ischemia ligation model eliminating collateralization of the deep femoral artery showed decreased reperfusion in *Arnt*^{SMKO} mice, implicating dysregulation of smaller vessels in impaired perfusion recovery (Figure S2). To assess for differences in angiogenesis, gastrocnemius sections were collected 7 days after ligation. Capillary number was evaluated by staining for CD31^{+} ECs, and the presence or absence of blood flow in each vessel was assessed by intravenous lectin injection before tissue collection (Figure 4A). At baseline, the unligated limbs of *Arnt*^{SMKO} and *Arnt*$^{lox/lox}$ show equivalent capillary densities and fractional perfusion (Figure 4B through 4D). At day 7, similar capillary and perfused vessel densities in ligated limbs of *Arnt*$^{lox/lox}$ and *Arnt*^{SMKO} mice were also observed (Figure 4B through 4D). In the ligated limbs, total number of capillaries in a 301-μm^2 area

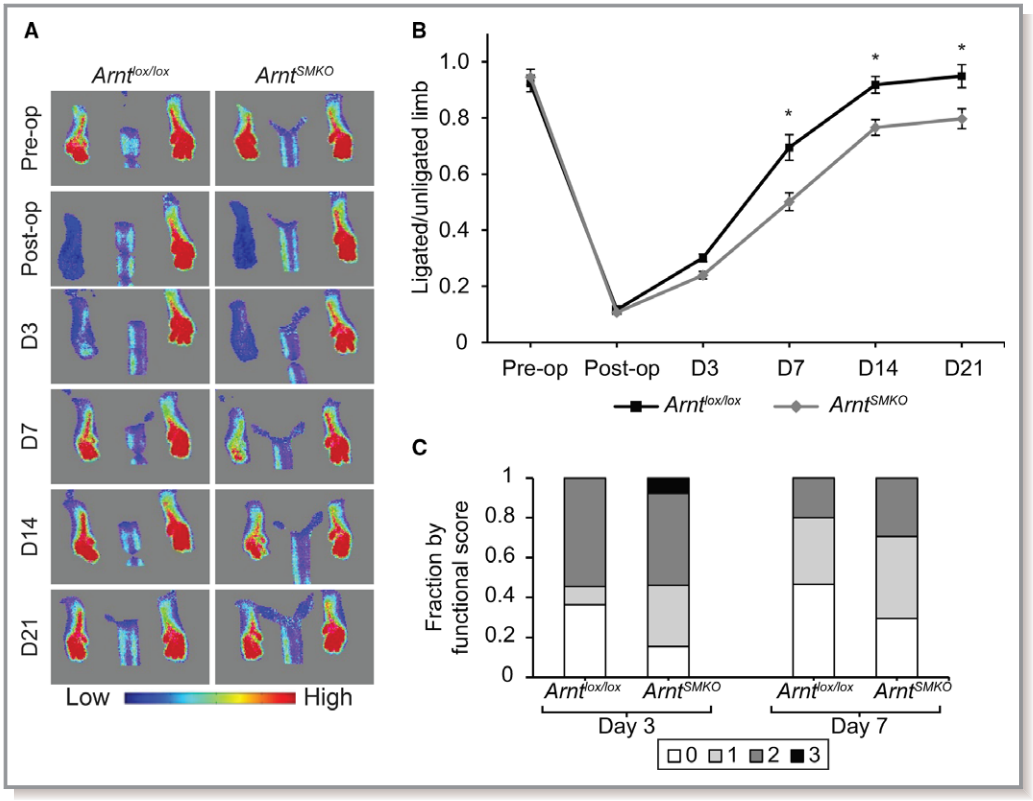

Figure 2. Bulk perfusion and functional recovery are reduced in *Arnt*^{SMKO} mice after femoral artery ligation. Ligations distal to the deep femoral artery branch point were performed in the left limbs of age- and sex-matched adult *Arnt*^{SMKO} and *Arnt*$^{lox/lox}$ mice. A, Representative images of perfusion measured using infrared laser Doppler scanning for *Arnt*^{SMKO} and *Arnt*$^{lox/lox}$ mice over 21-day recovery. B, Perfusion, reported as a ratio of ligated/unligated limb, was significantly lower in *Arnt*^{SMKO} compared with *Arnt*$^{lox/lox}$ mice from days 7 through 21 (n≥10, repeated-measures ANOVA). C, Functional scoring on days 3 and 7 shows impairment trend in functional recovery in *Arnt*^{SMKO} mice (n=11). D indicates day; Pre-op, preoperatively; Post-op, postoperatively. *P<0.05, *Arnt*^{SMKO} vs *Arnt*$^{lox/lox}$.

is not significantly different between *Arnt*$^{lox/lox}$ and *Arnt*^{SMKO} mice (Figure 4B). Although there is a decrease in the number of CD31^{+} capillaries/myocyte in the ligated limb of *Arnt*$^{lox/lox}$ and *Arnt*^{SMKO} mice relative to their counterpart unligated limb, it is only statistically significant in *Arnt*^{SMKO} mice (Figure 4C). In contrast, fractional perfusion of capillaries is significantly decreased in the ligated relative to unligated limbs in both *Arnt*^{SMKO} and *Arnt*$^{lox/lox}$ mice (Figure 4D). Sections from unligated and ligated limbs were stained with SMA to identify smooth muscle cells associated with any identified CD31^{+} capillaries. Unligated and day 7 sections exhibited little colocalization of SMA with capillaries (Figure S3).

Because the bulk of angiogenic responses is known to occur between days 7 and 28 after femoral artery ligation, capillary density was also measured at day 28 to thoroughly assess for effects of *Arnt* deficiency on angiogenesis. Quantified by average capillaries/301 μm^2, both *Arnt*$^{lox/lox}$ and *Arnt*^{SMKO} mice have increased numbers of capillaries in the day 28 ligated relative to unligated gastrocnemius muscles (Figure 4F); however, when capillaries per myocyte were quantified, the smaller myocytes of *Arnt*^{SMKO} ligated gastrocnemius muscles reveal a deficiency in late angiogenic responses. Although *Arnt*$^{lox/lox}$ shows recovery in the number of capillaries per myocyte by day 28, *Arnt*^{SMKO} recovery is limited, with significantly reduced capillary/myocyte ratios in ligated limbs (Figure 4E and 4G). No difference was apparent at day 28 in frequency of SMA^{+} CD31^{+} vessels between ligated *Arnt*^{SMKO} and *Arnt*$^{lox/lox}$ limbs (Figure 4E and 4H). To comprehensively evaluate for variability in regional vascularization as recently shown by Schaad et al,[41] we assessed vascularity in 6 distinct regions across the gastrocnemius muscle. Numbers of capillaries and perfused vessels between *Arnt*^{SMKO} and *Arnt*$^{lox/lox}$ mice were comparable in all 6 regions at days 7 and 28 (Figure S4). In summary, although angiogenic deficiencies in *Arnt*^{SMKO} may contribute to late (day 14–28) perfusion plateau, similar angiogenic patterns and use of capillary beds are seen in both *Arnt*^{SMKO} and *Arnt*$^{lox/lox}$ mice at day 7 after femoral artery ligation.

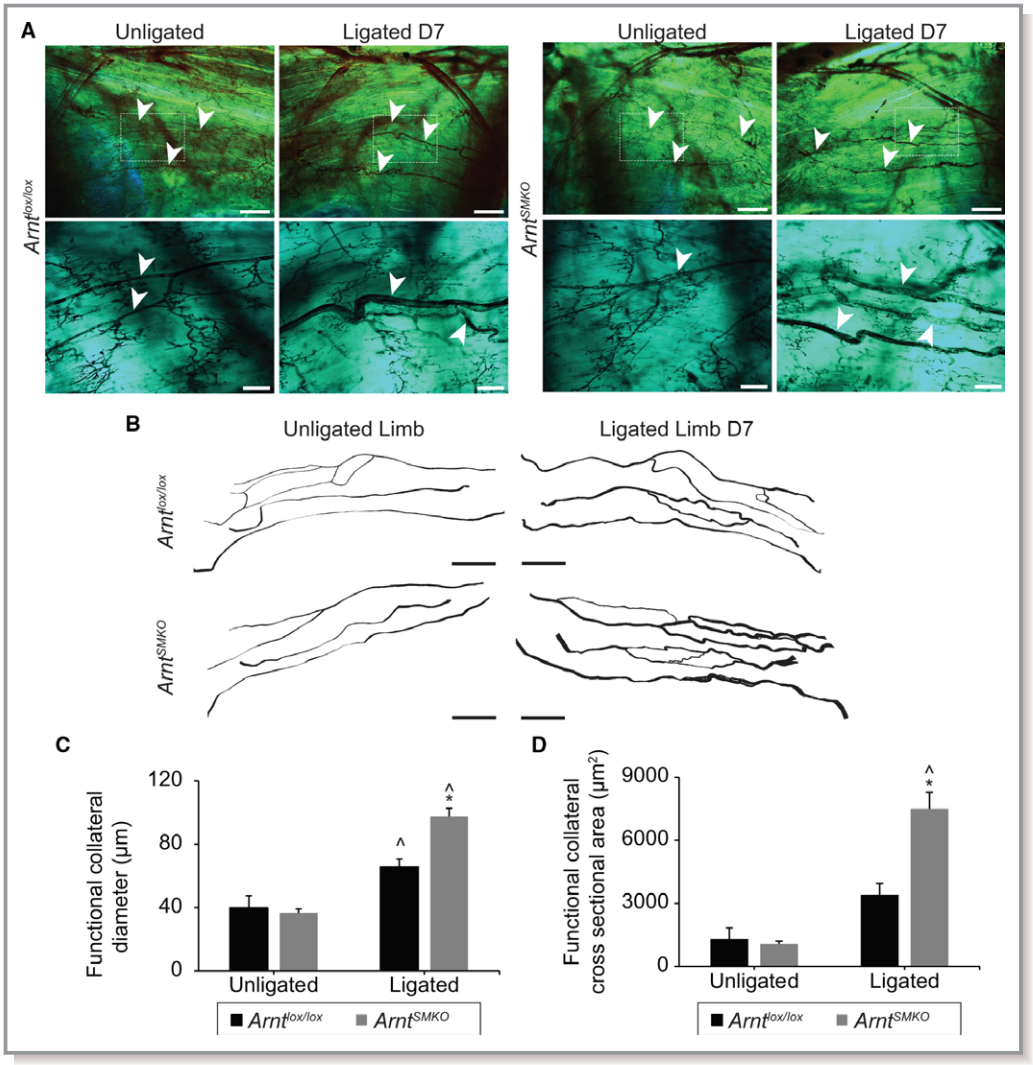

Figure 3. Vascular smooth muscle cell aryl hydrocarbon receptor nuclear translocator (ARNT) is not required for ischemia-induced collateralization. Collateral vessel responses in adductor muscles visualized with pigment perfusion angiography at day 7. A, Lumen diameter enlargement visible in ligated compared with respective unligated limbs of *Arnt*^{SMKO} and *Arnt*$^{lox/lox}$ mice. The ×10 images in top rows illustrate similar patterning; arrowheads indicate collaterals of interest. Higher-magnification inset outlined by dashed rectangle. Scale bar=1 mm. The ×65 images in bottom rows captured through green fluorescent protein filter for improved contrast. Scale bar=250 μm. B, Tracings of skeletonized images across entire length of collaterals. Scale bar=1 mm. C, Average collateral diameters show dilation in ligated limbs of both *Arnt*^{SMKO} and *Arnt*$^{lox/lox}$ mice. Collaterals in *Arnt*^{SMKO} ligated limbs are significantly larger than in *Arnt*$^{lox/lox}$ (n=3). D, Cross-sectional area calculations reflect approximation of projected flow rate. Measurements indicate 2.5-fold larger collateral vessels in *Arnt*^{SMKO} relative to *Arnt*$^{lox/lox}$ mice (n=3). 1-way ANOVAs were performed. D indicates day. *P<0.05, *Arnt*^{SMKO} vs *Arnt*$^{lox/lox}$; ^P<0.05, ligated vs unligated.

Arnt^{SMKO} Mice Show Increased Hypoxia and Damage in Gastrocnemius Muscle in Response to Ischemia

To assess the anatomical consequences of perfusion deficit, gastrocnemius muscle cross sections were stained with hematoxylin and eosin. Although *Arnt*^{SMKO} and *Arnt*$^{lox/lox}$ unligated limbs displayed normal skeletal muscle histological features, striking differences were observed between ligated limbs at day 7 (Figure 5A and 5B). Disruption of the muscular structure, defined by centrally located nuclei, decreased myocyte diameter, and abundant infiltrating cells were prominent features in *Arnt*^{SMKO} tissues, whereas *Arnt*$^{lox/lox}$ tissues were relatively unaffected (Figure 5A). At day 28 after femoral artery ligation, centralized nuclei and evidence of regenerating myocytes were still visible in *Arnt*^{SMKO} gastrocnemius sections

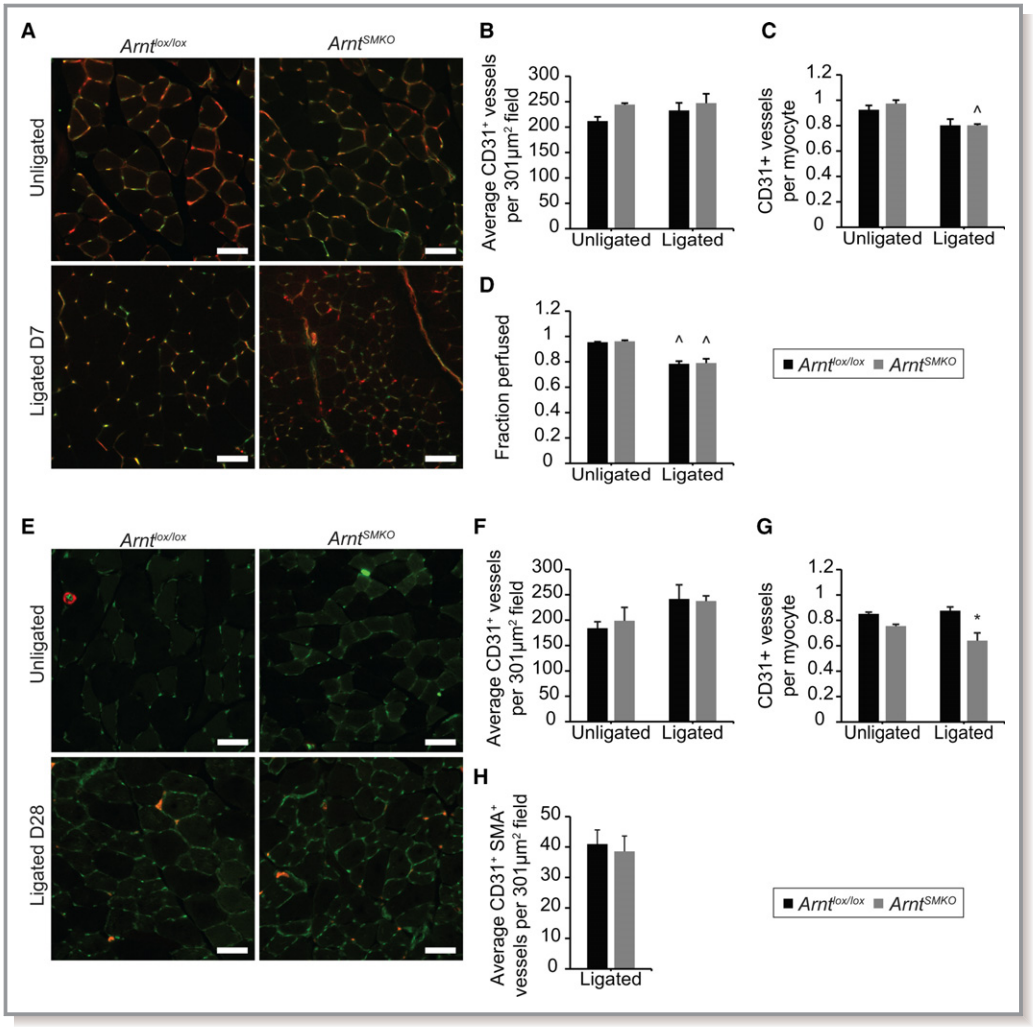

Figure 4. Histological assessment of capillary number and perfusion status in gastrocnemius muscle (GC). A, Representative micrographs of perfused vessels assessed by staining sections for CD31 (green) from GCs processed after mice were infused with endothelium-binding intravenous lectin at day 7 after femoral artery ligation (red). Although the number of $CD31^+$ capillaries per field at day 7 is not significantly different (B), ligated limbs of $Arnt^{SMKO}$ and $Arnt^{lox/lox}$ mice show decreased $CD31^+$ capillaries/myocyte (C) and fraction of perfused double-positive vessels (D) compared with unligated limbs at day 7 (n=4). No significant differences were seen between $Arnt^{SMKO}$ and $Arnt^{lox/lox}$ in any of the above metrics at day 7. E, Representative images of immunostained sections for CD31-labeled vessels (green) and α-smooth muscle actin (SMA; smooth muscle cells; red) from day 28 after ligation of GCs. F, Numbers of $CD31^+$ capillaries per field in day 28 ligated limbs of $Arnt^{SMKO}$ and $Arnt^{lox/lox}$ are similar to, if not increased, over unligated limbs (n=3). G, Ligated limbs of $Arnt^{SMKO}$ mice show decreased $CD31^+$ capillaries/myocyte compared with ligated limbs of $Arnt^{lox/lox}$ mice at day 28 (n=3). Scale bar=50 μm. H, Day 28 ligated limbs of $Arnt^{SMKO}$ and $Arnt^{lox/lox}$ have similar numbers of $CD31^+$ SMA^+ vessels (n=3). One-way ANOVA (B), Kruskal-Wallis test (C, D, F, and G), or unpaired 2-tailed *t* test (H) was used. D indicates day. $^*P<0.05$, $Arnt^{SMKO}$ vs $Arnt^{lox/lox}$; $^{\wedge}P<0.05$, ligated vs unligated.

(Figure 5A). Across the gastrocnemius muscle, these pathologic features extend over >60% of the ligated limbs of $Arnt^{SMKO}$ mice compared with <30% of the area of $Arnt^{lox/lox}$ gastrocnemius muscle (Figure 5B and 5C). Overall, the histological features reflect a maladaptive injury response, consistent with chronically reduced blood flow recovery in $Arnt^{SMKO}$ mice.

At the tissue level, hypoxia identifies areas of limited perfusion; thus, to quantify the extent of hypoxic gastrocnemius muscle after femoral artery ligation, pimonidazole intraperitoneal injection was used to label hypoxic tissues. Pimonidazole adducts, which identify tissue with <10 mm Hg O_2, were neither found in gastrocnemius sections from unligated limbs of $Arnt^{SMKO}$ and $Arnt^{lox/lox}$ mice nor present in $Arnt^{lox/lox}$ sections at day 7 (Figure 5D).[42,43] However, large hypoxic pimonidazole$^+$ areas were present in ligated limbs of $Arnt^{SMKO}$ mice 7 days after ligation (Figure 5D

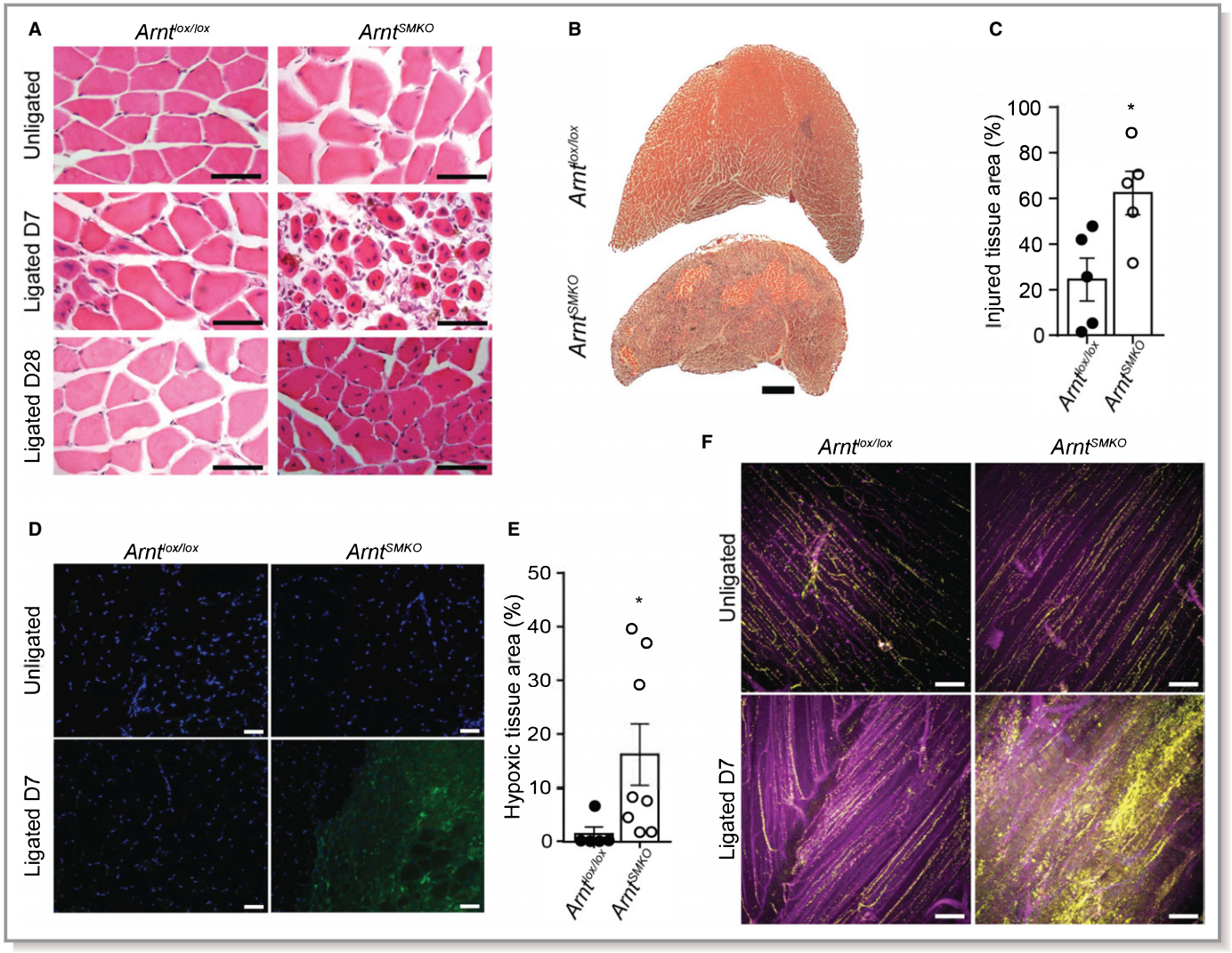

Figure 5. Ischemic skeletal muscle regeneration and vessel integrity are impaired in *Arnt*^{SMKO} mice. A, Representative images of hematoxylin and eosin–stained gastrocnemius muscle (GC) sections show comparable muscle phenotype in unligated limbs. Day 7 assessment illustrates widespread atrophic myocytes and infiltrating cells in *Arnt*^{SMKO} while present only in small well-defined areas of *Arnt*$^{lox/lox}$ GCs. Signs of damage and delayed regeneration, including centralized nuclei, persist to day 28 in *Arnt*^{SMKO} mice (n=3). Scale bar=50 μm. B and C, Whole GC cross sections show increased tissue damage in *Arnt*^{SMKO} compared with *Arnt*$^{lox/lox}$ in ligated limbs at day 7 (n=5). Scale bar=500 μm. Histological analysis (D) and quantification (E) of *Arnt*^{SMKO} ligated limbs show an increase in hypoxic regions identified by pimonidazole (Hypoxyprobe; green) staining at day 7 that are absent from unligated limbs of *Arnt*^{SMKO} and either limb of *Arnt*$^{lox/lox}$, with 4′,6-diamidino-2-phenylindole (blue; nuclei counterstain; n≥5). Scale bar=50 μm. F, Representative multiphoton images of fluorescein-conjugated dextran (yellow) administered intravenously show increased permeability in ligated limbs of *Arnt*^{SMKO} mice at day 7. CD31^{+} vessels (purple; n=2). Scale bar=100 μm. Unpaired 2-tailed *t* test (C) or Mann-Whitney test (E) was used. D indicates day. **P*<0.05, *Arnt*^{SMKO} vs *Arnt*$^{lox/lox}$.

and 5E). Together, significantly increased tissue damage and hypoxic areas demonstrate that loss of VSMC ARNT leads to substantial skeletal muscle injury after induced HLI.

Next, vascular integrity was examined by evaluating permeability to intravenous infused high-molecular-weight FITC-dextran. In both gastrocnemius muscles of *Arnt*$^{lox/lox}$ and the unligated limb of *Arnt*^{SMKO}, dextran was limited to CD31^{+} vascular structures in thick coronal sections imaged by multiphoton microscopy; however, extravascular dextran infiltrates were diffusely present in gastrocnemius muscles of *Arnt*^{SMKO} ligated limbs (Figure 5F). Collectively, increased tissue damage, hypoxic areas, and vascular permeability suggest that compromised vasculature in *Arnt*^{SMKO} underlies impaired perfusion and skeletal muscle injury after induced HLI.

Altered Vascular Smooth Muscle Morphologic Features in *Arnt*^{SMKO} Mice

Despite substantial collateralization and similar capillary responses in the first week after ligation, the presence of significant and persistent perfusion deficits and tissue

disruption point to a smooth muscle effect outside of these classically endothelial-driven perfusion restoration mechanisms. In light of recent reports of aberrant arteriolar VSMC wrapping in dysfunctional vasculature,[44] we examined the cellular architecture of arterioles using whole mount confocal fluorescent microscopy imaging of skeletal muscle samples. Visualization of α-SMA$^+$ arterioles revealed striking differences in VSMC morphologic features and conduit coverage in native spinotrapezius muscle tissue from *Arnt*^{SMKO} versus *Arnt*$^{lox/lox}$ mice (Figure 6A). Although the *Arnt*$^{lox/lox}$ VSMCs appear well organized and tightly wrapped, with smooth coverage along the length of the vessel, the *Arnt*^{SMKO} VSMCs appeared more rounded, clearly delineated, and detached (Figure 6A and Figure S5). Similarly sized vessels were also examined deep in the gastrocnemius muscles by multiphoton microscopy. Morphologic disruption of SMA$^+$ VSMCs affected arterioles in ligated and unligated limbs of *Arnt*^{SMKO} mice (Figure 6B). The aberrant perimural morphologic features of arterioles in *Arnt*^{SMKO} mice implicate a dysregulated VSMC phenotype at the cellular level linked to impaired perfusion recovery.

Loss of ARNT Alters VSMC Phenotype

To assess ARNT's role in VSMC phenotype and responses to hypoxic stress in ischemic limbs, cultured aortic VSMCs from *Arnt*^{SMKO} and *Arnt*$^{lox/lox}$ mice were challenged with 24-hour hypoxic exposure at 2% O_2.[45,46] Evaluation of transcripts revealed divergent changes in drivers of hypoxia-induced phenotype modulation well described in pulmonary artery and aortic VSMCs (Figure 7).[20,47–52] Expression of HIF targets, vascular endothelial growth factor A (*Vegfa*) and glucose transporter 1 (*Glut1*), whose levels increase in hypoxia and are attenuated by ARNT deletion in ECs, responded as expected.[33,53–55] Hypoxia induced expression of *Vegfa* and *Glut1* in *Arnt*$^{lox/lox}$ VSMCs, and loss of ARNT prevented induction of expression in hypoxia (Figure 7A and 7B). Transcriptional changes were also observed in critical proliferative and migratory genes. *Arnt*^{SMKO} VSMCs displayed reduced expression of serpin family E member 1 (*Serpine1*; *Pai1*), fibroblast growth factor 2 (*Fgf2*), PDGF receptor β (*Pdgfr*β), *Pdgfb*, and tissue inhibitor of metalloproteinases 1 (*Timp1*) mRNA levels relative to normoxic *ArntSMKO* VSMCs and, except *Pdgfb*, relative to hypoxic *Arnt*$^{lox/lox}$ VSMCs (Figure 7C through 7G). Furthermore, differences in gene expression were observed under normoxia in *Arnt*^{SMKO} VSMCs, including increases in matrix metalloproteinase 3 (*Mmp3*) and decreases in *Vegfa*, *Glut1*, *Fgf2*, *Pdgfr*β, and thrombospondin-2 (*Thbs2*) relative to *Arnt*$^{lox/lox}$ VSMCs (Figure 7A, 7B, 7D, 7E, 7H, and 7J). Although hypoxic treatment of control VSMCs leads to reduced expression of thrombospondin-1 and thrombospondin-2 (*Thbs1* and *Thbs2*), *Arnt*^{SMKO} VSMCs failed to mitigate *Thbs2* reduction (Figure 7I and 7J). To examine the phenotypic consequences of transcriptional dysregulation, migration and proliferation were evaluated. Migration assessed by 2-dimensional scratch assay in the presence of PDGF-BB showed *Arnt*^{SMKO} cells are less migratory in hypoxia than *Arnt*$^{lox/lox}$ cultures (Figure 8A).

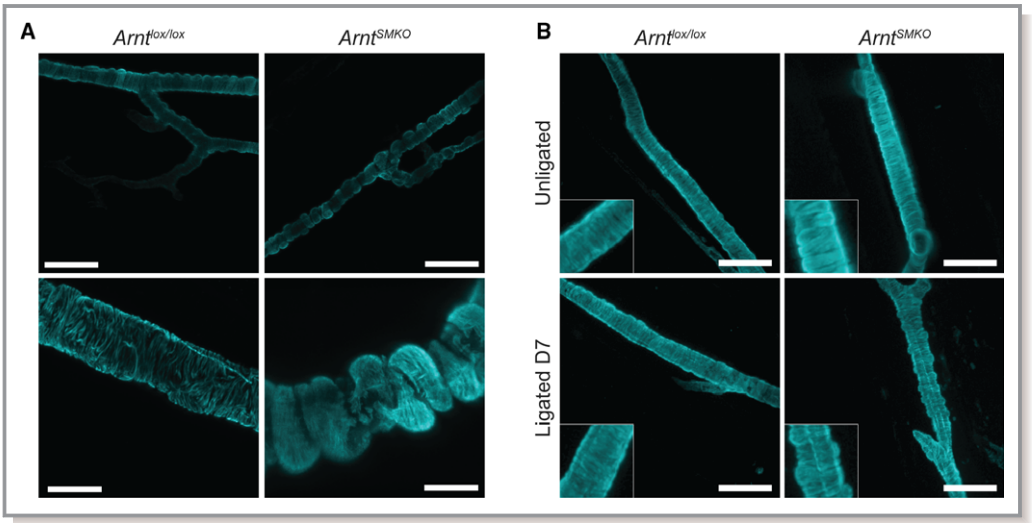

Figure 6. Smooth muscle morphologic features and perimural wrapping of small arterioles. A, Representative confocal images of smooth muscle actin positive (SMA$^+$; cyan) vascular smooth muscle cells (VSMCs) around small arterioles in spinotrapezius muscle illustrate disruption of organization and VSMC morphologic features in *Arnt*^{SMKO} mice (n=3). Top row scale bar=60 μm. Bottom row scale bar=10 μm. B, Representative peripheral arterioles in gastrocnemius muscles of *Arnt*^{SMKO} mice also display aberrant morphologic features and organization of SMA$^+$ VSMCs visualized by multiphoton microscopy (n=3). Scale bar=60 μm; insets, ×3 magnification. D indicates day.

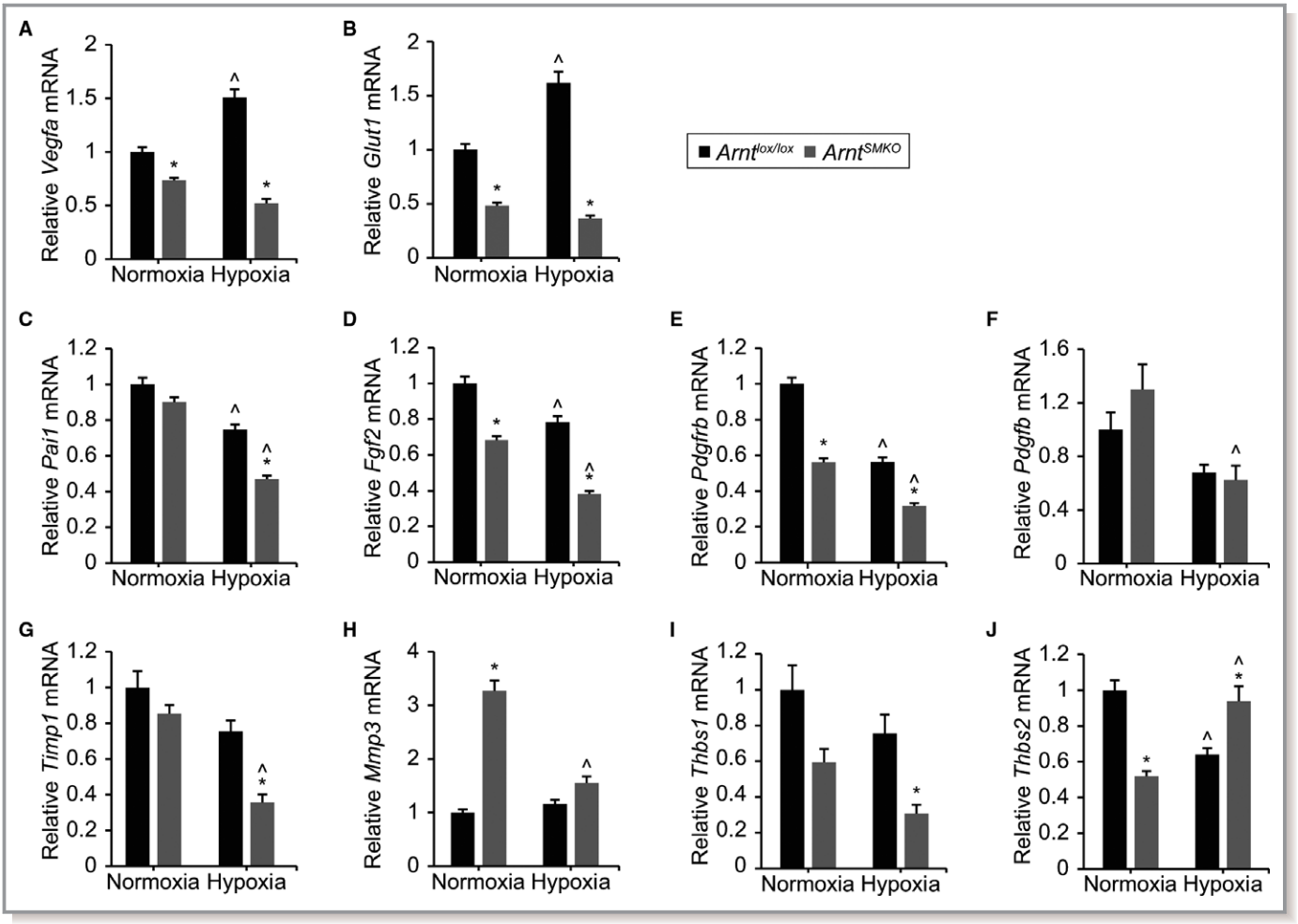

Figure 7. Transcriptional expression of proliferation and migration regulators in response to hypoxia. A through J, mRNA samples from *Arnt*^{SMKO} and *Arnt*$^{lox/lox}$ mouse aortic vascular smooth muscle cell (VSMC) cultures after 24 hours of hypoxia (2% O_2) exposure were analyzed by real-time quantitative polymerase chain reaction, normalized to *18s* ribosomal RNA, and compared with normoxic (21% O_2) control samples. Transcriptional profile of VSMCs from *Arnt*^{SMKO} differs from control *Arnt*$^{lox/lox}$ samples: *Vegfa* (A), *Glut1* (B), *Pai1* (*Serpine1*; C), *Fgf2* (D), *Pdgfr*b (E), *Pdgfb* (F), *Timp1* (G), *Mmp3* (H), *Thbs1* (I), and *Thbs2* (J). n=3. 1- way ANOVAs were performed. *P<0.05, *Arnt*^{SMKO} vs *Arnt*$^{lox/lox}$; ^P<0.05, hypoxia vs normoxia.

Proliferation, quantified by percentage of 5-bromo-2′-deoxyuridine–positive cells, increased when *Arnt*$^{lox/lox}$ cells were exposed to hypoxia for 24 hours (Figure 8B). *Arnt*^{SMKO} VSMCs show no increased proliferation in hypoxia over normoxia, but they notably have greater percentage of replicating cells than *Arnt*$^{lox/lox}$ under both conditions. Collectively, these findings suggest that gene expression differences in hypoxia-treated *Arnt*^{SMKO} VSMCs underlie cellular derangements responsible for vascular reperfusion impairment.

Discussion

The present study illustrates the importance of HIF-orchestrated VSMC responses in peripheral perfusion recovery in a model of induced HLI. Specifically, knockout of *Arnt* in smooth muscle impairs perfusion restoration after femoral artery ligation. Although insufficient blood flow manifests in increased hypoxic tissue and skeletal muscle damage in the ischemic limbs of *Arnt*^{SMKO} mice, interestingly there were no signs of limitation in collateral dilation or of disruption of perfused capillary density. However, loss of ARNT led to morphologic disorganization of VSMC coverage of small arterioles and increased vascular permeability in ligated limbs. Furthermore, the transcriptional dysregulation of multiple genes involved in VSMC function affect proliferation and migration of isolated *Arnt*^{SMKO} cells. In all, this study identifies hypoxia-mediated responses in VSMCs critical to maintaining VSMC phenotype, cellular organization around arterioles, and vessel integrity, and to achieving optimal reperfusion of ischemic peripheral tissues.

Our observation of impaired limb recovery with diminished reperfusion is striking in a mouse genetic model targeting

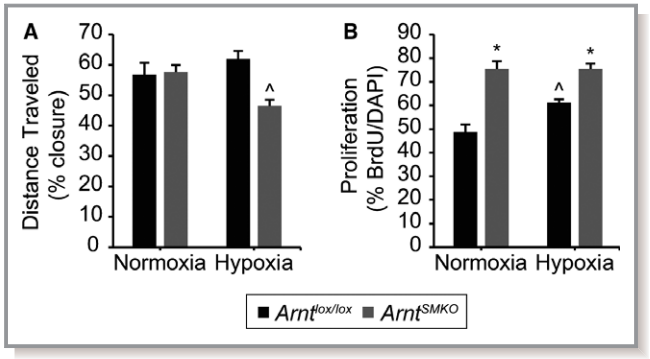

Figure 8. Assessment of vascular smooth muscle cell (VSMC) phenotype in vitro. A, Migration in normoxic (21% O_2) or hypoxic (2% O_2) conditions was detected in a 2-dimensional scratch assay measured after 6.5 hours. *Arnt*^{SMKO} VSMCs show decreased migration in hypoxia compared with *Arnt*$^{lox/lox}$ cultures (n=9). B, Quantitative analyses of immunopositive 5-bromo-2′-deoxyuridine (BrdU) cells reveal increased proliferation of *Arnt*^{SMKO} VSMCs in normoxia and hypoxia (n=3). 1- way ANOVAs were performed. DAPI indicates 4′,6-diamidino-2-phenylindole. *P<0.05, *Arnt*^{SMKO} vs *Arnt*$^{lox/lox}$; ^P<0.05, hypoxia vs normoxia.

smooth muscle cells. ECs have been described as the primary regulators of blood flow and orchestrators of reperfusion; however, the degree of impairment observed in *Arnt*^{SMKO} mice is more profound than that seen in global *Hif-1*$\alpha^{+/-}$ mice[23] and on par with endothelial-specific deletions of *Hif-2*α.[27] Furthermore, our findings are supported by a recent report of decreased reperfusion with *Hif-1*α deletion in VSMCs using a severe form of HLI.[28] Our genetic model conditionally deleting VSMC-ARNT permits efficient study of all HIF-canonical transcriptional function, whereas HIF-α subunit activities involving noncanonical binding partners remain undisrupted.[56] In context, our results demonstrate the importance of smooth muscle cell canonical HIF-dependent responses in perfusion recovery necessitated by regional peripheral ischemia.

Perfusion deficits in HLI models are often explained by impaired angiogenic and/or arteriogenic responses.[57] Classically, hemodynamic changes prompt arteriogenesis assessed by number and dilation of collaterals, whereas hypoxia drives angiogenesis visualized by increased capillary density; however, local stabilization of HIF-1α through introduction of a constitutively active variant or by inhibition of its degradation pathway increases both angiogenic and arteriogenic responses.[25,50,58,59] The impacts on reperfusion mechanisms are not explicitly described in *Hif-1*$\alpha^{+/-}$ or tissue-specific HIF-1α models, but endothelial-specific deletion of *Hif-2*α impairs both benchmark vascular remodeling processes.[27] Lower capillary density in day 28 *Arnt*^{SMKO} gastrocnemius muscles helps to explain the persisting perfusion limitations after recovery has plateaued. Yet, at day 7, when the perfusion deficit is largest, measurements of arteriogenesis and angiogenesis in response to HLI are similar in *Arnt*^{SMKO} and *Arnt*$^{lox/lox}$ mice. In fact, ligated limbs of *Arnt*^{SMKO} mice have larger-diameter collateral vessels at day 7 than their littermate controls. The inverse correlation between collateral cross-sectional area and bulk perfusion in *Arnt*^{SMKO} and *Arnt*$^{lox/lox}$ limbs suggests that collateral vessel diameter is responsive to changes in blood flow and compensating for elevated ischemia in mutant mice. In a model that spares HIF signaling in the endothelium, traditionally viewed as the primary driver of vascular ischemic responses, it may therefore be unremarkable that these processes appear intact.[60] Despite substantial arteriogenic and angiogenic responses, these compensatory changes are insufficient to restore perfusion to the affected tissue in the *Arnt*^{SMKO} mice. Whether attributable to greater extent of ischemic insult, injury, and/or impaired recovery, substantial areas of hypoxia remain at least 7 days after ligation and signs of tissue damage persist across the gastrocnemius muscle after 28 days of recovery. These findings suggest that established responses to ischemia through well-defined revascularization mechanisms do not adequately explain the perfusion deficit at day 7. Indeed, although increases in microvessel number have also been documented in affected peripheral tissues from patients with chronic limb ischemia, these responses also do not appear to be sufficient to alleviate ischemia.[22]

Perfusion, as measured by laser Doppler, can be described as a function of red blood cell concentration and flow rate.[61] In the absence of differences in cardiovascular function, global volumetric flow rates should be comparable in *Arnt*^{SMKO} and *Arnt*$^{lox/lox}$ mice. Thus, the perfusion deficit can be attributed to local changes in vascular flow rate in the hind limb. Recent reports of pathologic vessel patterning in regenerated vascular networks after HLI could clarify the *Arnt*^{SMKO} reperfusion deficit. Arpino et al implicated disordered VSMC phenotype and wrapping around small arterioles in limiting red blood cell transit through the microvasculature of regenerating skeletal muscle.[44] Similarly, in skeletal muscle of *Arnt*^{SMKO} mice, we detect aberrant smooth muscle cell morphologic features and investment of the small arterioles, consistent with these novel reports. Furthermore, the integrity of the microvasculature is compromised, as evidenced by increased permeability. Vascular leak affects pressure gradients and contributes to disruption of local blood flow. Thus, although the hallmark revascularization measurements (namely, collateral diameter, capillary number, and fractional perfusion) appear normal, disruption in VSMC patterning in vessels of *Arnt*^{SMKO} mice likely contributes to reduced reperfusion and muscle recovery after HLI.

In the pulmonary circulation, HIF-1 is a well-described mediator of hypoxia-triggered vascular remodeling and VSMC phenotype modulation. Mouse models of chronic hypoxia induced pulmonary hypertension with reduced HIF-1α activity, through either global haplodeficiency or SMC-specific

deletion, demonstrate decreased vascular remodeling.[17,62,63] Mature VSMCs retain a remarkable amount of plasticity and can exhibit a phenotypic spectrum ranging from principally contractile and rarely dividing to highly synthetic, proliferative, and migratory.[64] Early debate in the field about VSMC responses to hypoxia emerged in studies using pulmonary artery SMC cultures.[65] However, recent reports of pulmonary artery SMCs consistently show HIF-mediated hypoxic responses increase proliferation, survival, and migration, and stimulate growth factor production, including vascular endothelial growth factor A.[47–50] HIF targets, including PDGFs and fibroblast growth factors, are key promoters of VSMC proliferation and migration; their inhibition impairs proliferation of pulmonary artery SMCs in vitro and prevents vascular remodeling in models of pulmonary hypertension.[66,67] Expression of multiple HIF targets in $Arnt^{SMKO}$ VSMCs diverges from levels seen in control cells. Failure to maintain expression levels of *Pdgfr*β, *Pdgfb*, and *Fgf2* indicates dysregulation of pathways central to proliferative and migratory responses to hypoxia. Indeed, $Arnt^{SMKO}$ cells do not show proliferation increase with hypoxic exposure over normoxia and are less migratory than $Arnt^{lox/lox}$ in hypoxia.

Although these effects of HIF-dependent phenotypic modulation are varied in differing oxygenation and hemodynamic environments outside of the pulmonary circulation, several recent reports have identified HIF-1 as central to maintaining the structure and function of the arterial wall.[20,21,68] Downstream HIF-1 targets have been identified as important in systemic VSMC physiological features and response to hypoxic stimuli.[20,51,52] HIF targets, PDGF and thrombospondin-2, regulate VSMC attachment to extracellular matrix; impaired expression of *Pdgfr*β and *Thbs2* in $Arnt^{SMKO}$ helps explain disrupted VSMC morphologic features observed around arterioles.[69,70] As supporting cells in the vascular wall, it is well recognized that VSMCs are involved in physiologic responses to mechanical and biochemical changes in blood vessels. Changes in VSMC phenotype have consequences for vasoreactivity. Tissue-specific deletion of HIF-1α has been shown to increase contractility, a putative marker of mature VSMC phenotype, in studies of aortic and pulmonary artery VSMCs.[18,21,71] The morphologic changes in VSMCs around small arterioles in $Arnt^{SMKO}$ mice, taken together with the abnormal proliferative and migratory behavior and the altered gene expression observed in isolated cells, are consistent with phenotypic dysregulation of VSMCs.

In summary, the present study indicates that loss of hypoxic signals in VSMCs limits the ability of mice to recover from inducible HLI, a classic model for peripheral vascular disease. We provide evidence that, despite conventional compensatory arteriogenic and angiogenic responses in the first week after ligation, dysregulated smooth muscle cell function in $Arnt^{SMKO}$ arterioles, manifested by morphologic disruption, aberrant expression of key phenotypic regulators, and altered proliferation and migration, is sufficient to compromise vascular integrity and ultimately impair limb reperfusion. Our results therefore underscore a critical role for VSMC HIF in peripheral perfusion recovery and reiterate the importance of understanding the regulation of VSMC function in arteriolar vessels in supporting optimal blood flow.

Acknowledgments

We thank Alla Gomer, Keiki Sugi, Stephanie Lapping, and Alice Jo for technical assistance.

Sources of Funding

Funding for this work was provided by the National Institutes of Health F30 HL127985 (Borton), RO1 HL128281 (Proweller and Ramirez-Bergeron), RO1 HL096597 (Ramirez-Bergeron), T32 HL105338 (Borton and Alaiti), T32 GM7250 (Borton and Benson), TL1 RR024991 (Borton and Benson), F31 NS096857 (Benson), T32 NS077888 (Benson), and R25 HL103152 (Saunders).

Disclosures

None.

References

1. Fowkes FG, Rudan D, Rudan I, Aboyans V, Denenberg JO, McDermott MM, Norman PE, Sampson UK, Williams LJ, Mensah GA, Criqui MH. Comparison of global estimates of prevalence and risk factors for peripheral artery disease in 2000 and 2010: a systematic review and analysis. *Lancet*. 2013;382:1329–1340.
2. Carmeliet P. Mechanisms of angiogenesis and arteriogenesis. *Nat Med*. 2000;6:389–395.
3. Fischer C, Schneider M, Carmeliet P. Principles and therapeutic implications of angiogenesis, vasculogenesis and arteriogenesis. In: Moncada S, Higgs A, eds. *The Vascular Endothelium II*. Berlin, Heidelberg: Springer; 2006:157–212.
4. Cooke JP, Losordo DW. Modulating the vascular response to limb ischemia. *Circ Res*. 2015;116:1561–1578.
5. Schwartz SM, Campbell GR, Campbell JH. Replication of smooth muscle cells in vascular disease. *Circ Res*. 1986;58:427–444.
6. Welsh DJ, Peacock AJ. Cellular responses to hypoxia in the pulmonary circulation. *High Alt Med Biol*. 2013;14:111–116.
7. Iyer NV, Kotch LE, Agani F, Leung SW, Laughner E, Wenger RH, Gassmann M, Gearhart JD, Lawler AM, Yu AY, Semenza GL. Cellular and developmental control of O_2 homeostasis by hypoxia-inducible factor 1 alpha. *Genes Dev*. 1998;12:149–162.
8. Maltepe E, Schmidt JV, Baunoch D, Bradfield CA, Simon MC. Abnormal angiogenesis and responses to glucose and oxygen deprivation in mice lacking the protein ARNT. *Nature*. 1997;386:403–407.
9. Peng J, Zhang L, Drysdale L, Fong GH. The transcription factor EPAS-1/hypoxia-inducible factor 2alpha plays an important role in vascular remodeling. *Proc Natl Acad Sci U S A*. 2000;97:8386–8391.
10. Tian H, Hammer RE, Matsumoto AM, Russell DW, McKnight SL. The hypoxia-responsive transcription factor EPAS1 is essential for catecholamine homeostasis and protection against heart failure during embryonic development. *Genes Dev*. 1998;12:3320–3324.
11. Compernolle V, Brusselmans K, Acker T, Hoet P, Tjwa M, Beck H, Plaisance S, Dor Y, Keshet E, Lupu F, Nemery B, Dewerchin M, Van Veldhoven P, Plate K, Moons L, Collen D, Carmeliet P. Loss of HIF-2alpha and inhibition of VEGF

impair fetal lung maturation, whereas treatment with VEGF prevents fatal respiratory distress in premature mice. *Nat Med*. 2002;8:702–710.

12. Ramirez-Bergeron DL, Simon MC. Hypoxia-inducible factor and the development of stem cells of the cardiovascular system. *Stem Cells*. 2001;19:279–286.
13. Giaccia AJ, Simon MC, Johnson R. The biology of hypoxia: the role of oxygen sensing in development, normal function, and disease. *Genes Dev*. 2004;18:2183–2194.
14. Andrikopoulou E, Zhang X, Sebastian R, Marti G, Liu L, Milner SM, Harmon JW. Current insights into the role of HIF-1 in cutaneous wound healing. *Curr Mol Med*. 2011;11:218–235.
15. Jain S, Maltepe E, Lu MM, Simon C, Bradfield CA. Expression of ARNT, ARNT2, HIF1α, HIF2α and Ah receptor mRNAs in the developing mouse. *Mech Dev*. 1998;73:117–123.
16. Pawlus MR, Hu CJ. Enhanceosomes as integrators of hypoxia inducible factor (HIF) and other transcription factors in the hypoxic transcriptional response. *Cell Signal*. 2013;25:1895–1903.
17. Ball MK, Waypa GB, Mungai PT, Nielsen JM, Czech L, Dudley VJ, Beussink L, Dettman RW, Berkelhamer SK, Steinhorn RH, Shah SJ, Schumacker PT. Regulation of hypoxia-induced pulmonary hypertension by vascular smooth muscle hypoxia-inducible factor-1alpha. *Am J Respir Crit Care Med*. 2014;189:314–324.
18. Kim YM, Barnes EA, Alvira CM, Ying L, Reddy S, Cornfield DN. Hypoxia-inducible factor-1alpha in pulmonary artery smooth muscle cells lowers vascular tone by decreasing myosin light chain phosphorylation. *Circ Res*. 2013;112:1230–1233.
19. Shimoda LA, Laurie SS. Vascular remodeling in pulmonary hypertension. *J Mol Med (Berl)*. 2013;91:297–309.
20. Imanishi M, Tomita S, Ishizawa K, Kihira Y, Ueno M, Izawa-Ishizawa Y, Ikeda Y, Yamano N, Tsuchiya K, Tamaki T. Smooth muscle cell specific Hif-1alpha deficiency suppresses angiotensin II-induced vascular remodeling in mice. *Cardiovasc Res*. 2014;102:460–468.
21. Huang Y, Di Lorenzo A, Jiang W, Cantalupo A, Sessa WC, Giordano FJ. Hypoxia-inducible factor-1alpha in vascular smooth muscle regulates blood pressure homeostasis through a peroxisome proliferator-activated receptor-gamma-angiotensin II receptor type 1 axis. *Hypertension*. 2013;62:634–640.
22. Ho TK, Rajkumar V, Ponticos M, Leoni P, Black DCM, Abraham DJ, Baker DM. Increased endogenous angiogenic response and hypoxia-inducible factor-1a in human critical limb ischemia. *J Vasc Surg*. 2006;43:125–133.
23. Bosch-Marce M, Okuyama H, Wesley JB, Sarkar K, Kimura H, Liu YV, Zhang H, Strazza M, Rey S, Savino L, Zhou YF, McDonald KR, Na Y, Vandiver S, Rabi A, Shaked Y, Kerbel R, LaVallee T, Semenza GL. Effects of aging and hypoxia-inducible factor-1 activity on angiogenic cell mobilization and recovery of perfusion after limb ischemia. *Circ Res*. 2007;101:1310–1318.
24. Li M, Liu C, Bin J, Wang Y, Chen J, Xiu J, Pei J, Lai Y, Chen D, Fan C, Xie J, Tao Y, Wu P. Mutant hypoxia inducible factor-1alpha improves angiogenesis and tissue perfusion in ischemic rabbit skeletal muscle. *Microvasc Res*. 2011;81:26–33.
25. Patel TH, Kimura H, Weiss CR, Semenza GL, Hofmann LV. Constitutively active HIF-1alpha improves perfusion and arterial remodeling in an endovascular model of limb ischemia. *Cardiovasc Res*. 2005;68:144–154.
26. Milkiewicz M, Pugh CW, Egginton S. Inhibition of endogenous HIF inactivation induces angiogenesis in ischaemic skeletal muscles of mice. *J Physiol*. 2004;560:21–26.
27. Skuli N, Majmundar AJ, Krock BL, Mesquita RC, Mathew LK, Quinn ZL, Runge A, Liu L, Kim MN, Liang J, Schenkel S, Yodh AG, Keith B, Simon MC. Endothelial HIF-2alpha regulates murine pathological angiogenesis and revascularization processes. *J Clin Invest*. 2012;122:1427–1443.
28. MacLauchlan SC, Calabro NE, Huang Y, Krishna M, Bancroft T, Sharma T, Yu J, Sessa WC, Giordano F, Kyriakides TR. HIF-1alpha represses the expression of the angiogenesis inhibitor thrombospondin-2. *Matrix Biol*. 2018;65:45–58.
29. Lepore JJ, Cheng L, Min LuM, Mericko PA, Morrisey EE, Parmacek MS. High-efficiency somatic mutagenesis in smooth muscle cells and cardiac myocytes in SM22alpha-Cre transgenic mice. *Genesis*. 2005;41:179–184.
30. Proweller A, Wright AC, Horng D, Cheng L, Lu MM, Lepore JJ, Pear WS, Parmacek MS. Notch signaling in vascular smooth muscle cells is required to pattern the cerebral vasculature. *Proc Natl Acad Sci U S A*. 2007;104:16275–16280.
31. Lu Y, Zhang L, Liao X, Sangwung P, Prosdocimo DA, Zhou G, Votruba AR, Brian L, Han YJ, Gao H, Wang Y, Shimizu K, Weinert-Stein K, Khrestian M, Simon DI, Freedman NJ, Jain MK. Kruppel-like factor 15 is critical for vascular inflammation. *J Clin Invest*. 2013;123:4232–4241.
32. Tomita S, Sinal CJ, Yim SH, Gonzalez FJ. Conditional disruption of the aryl hydrocarbon receptor nuclear translocator (Arnt) gene leads to loss of target gene induction by the aryl hydrocarbon receptor and hypoxia-inducible factor 1alpha. *Mol Endocrinol*. 2000;14:1674–1681.
33. Han Y, Yang K, Proweller A, Zhou G, Jain MK, Ramirez-Bergeron DL. Inhibition of ARNT severely compromises endothelial cell viability and function in response to moderate hypoxia. *Angiogenesis*. 2012;15:409–420.
34. Limbourg A, Korff T, Napp LC, Schaper W, Drexler H, Limbourg FP. Evaluation of postnatal arteriogenesis and angiogenesis in a mouse model of hind-limb ischemia. *Nat Protoc*. 2009;4:1737–1748.
35. Peng X, Wang J, Lassance-Soares RM, Najafi AH, Sood S, Aghili N, Alderman LO, Panza JA, Faber JE, Wang S, Epstein SE, Burnett MS. Gender differences affect blood flow recovery in a mouse model of hindlimb ischemia. *Am J Physiol Heart Circ Physiol*. 2011;300:H2027–H2034.
36. Bailey AM, O'Neill TJ, Morris CE, Peirce SM. Arteriolar remodeling following ischemic injury extends from capillary to large arteriole in the microcirculation. *Microcirculation*. 2008;15:389–404.
37. Muller PY, Janovjak H, Miserez AR, Dobbie Z. Processing of gene expression data generated by quantitative real-time RT-PCR. *Biotechniques*. 2002;32:1372–1374, 1376, 1378-1379.
38. Wenger RH. Cellular adaptation to hypoxia: O_2-sensing protein hydroxylases, hypoxia-inducible transcription factors, and O_2-regulated gene expression. *FASEB J*. 2002;16:1151–1162.
39. Salceda S, Beck I, Caro J. Absolute requirement of aryl hydrocarbon receptor nuclear translocator protein for gene activation by hypoxia. *Arch Biochem Biophys*. 1996;334:389–394.
40. Gao S, Ho D, Vatner DE, Vatner SF. Echocardiography in mice. *Curr Protoc Mouse Biol*. 2011;1:71–83.
41. Schaad L, Hlushchuk R, Barré S, Gianni-Barrera R, Haberthür D, Banfi A, Djonov V. Correlative imaging of the murine hind limb vasculature and muscle tissue by MicroCT and light microscopy. *Sci Rep*. 2017;7:41842.
42. Chou SC, Azuma Y, Varia MA, Raleigh JA. Evidence that involucrin, a marker for differentiation, is oxygen regulated in human squamous cell carcinomas. *Br J Cancer*. 2004;90:728–735.
43. Gross MW, Karbach U, Groebe K, Franko AJ, Mueller-Klieser W. Calibration of misonidazole labeling by simultaneous measurement of oxygen tension and labeling density in multicellular spheroids. *Int J Cancer*. 1995;61:567–573.
44. Arpino JM, Nong Z, Li F, Yin H, Ghonaim N, Milkovich S, Balint B, O'Neil C, Fraser GM, Goldman D, Ellis CG, Pickering JG. Four-dimensional microvascular analysis reveals that regenerative angiogenesis in ischemic muscle produces a flawed microcirculation. *Circ Res*. 2017;120:1453–1465.
45. Dormandy JA, Rutherford RB; TASC Working Group. TransAtlantic Inter-Society Consensus. Management of peripheral arterial disease. *J Vasc Surg*. 2000;31:S1–S296.
46. Browning E, Wang H, Hong N, Yu K, Buerk DG, DeBolt K, Gonder D, Sorokina EM, Patel P, De Leon DD, Feinstein SI, Fisher AB, Chatterjee S. Mechanotransduction drives post ischemic revascularization through K(ATP) channel closure and production of reactive oxygen species. *Antioxid Redox Signal*. 2014;20:872–886.
47. Schultz K, Fanburg BL, Beasley D. Hypoxia and hypoxia-inducible factor-1alpha promote growth factor-induced proliferation of human vascular smooth muscle cells. *Am J Physiol Heart Circ Physiol*. 2006;290:H2528–H2534.
48. Chanakira A, Kir D, Barke RA, Santilli SM, Ramakrishnan S, Roy S. Hypoxia differentially regulates arterial and venous smooth muscle cell migration. *PLoS One*. 2015;10:e0138587.
49. Deng B, Du J, Hu R, Wang AP, Wu WH, Hu CP, Li YJ, Li XH. MicroRNA-103/107 is involved in hypoxia-induced proliferation of pulmonary arterial smooth muscle cells by targeting HIF-1beta. *Life Sci*. 2016;147:117–124.
50. Kelly BD, Hackett SF, Hirota K, Oshima Y, Cai Z, Berg-Dixon S, Rowan A, Yan Z, Campochiaro PA, Semenza GL. Cell type-specific regulation of angiogenic growth factor gene expression and induction of angiogenesis in nonischemic tissue by a constitutively active form of hypoxia-inducible factor 1. *Circ Res*. 2003;93:1074–1081.
51. Osada-Oka M, Ikeda T, Akiba S, Sato T. Hypoxia stimulates the autocrine regulation of migration of vascular smooth muscle cells via HIF-1alpha-dependent expression of thrombospondin-1. *J Cell Biochem*. 2008;104:1918–1926.
52. Erdozain OJ, Pegrum S, Winrow VR, Horrocks M, Stevens CR. Hypoxia in abdominal aortic aneurysm supports a role for HIF-1α and Ets-1 as drivers of matrix metalloproteinase upregulation in human aortic smooth muscle cells. *J Vasc Res*. 2011;48:163–170.
53. Ramirez-Bergeron DL, Runge A, Adelman DM, Gohil M, Simon MC. HIF-dependent hematopoietic factors regulate the development of the embryonic vasculature. *Dev Cell*. 2006;11:81–92.
54. Ramirez-Bergeron DL, Runge A, Dahl KD, Fehling HJ, Keller G, Simon MC. Hypoxia affects mesoderm and enhances hemangioblast specification during early development. *Development*. 2004;131:4623–4634.
55. Maxwell PH, Dachs GU, Gleadle JM, Nicholls LG, Harris AL, Stratford IJ, Hankinson O, Pugh CW, Ratcliffe PJ. Hypoxia-inducible factor-1 modulates

gene expression in solid tumors and influences both angiogenesis and tumor growth. *Proc Natl Acad Sci U S A*. 1997;94:8104–8109.

56. Semenza GL. A compendium of proteins that interact with HIF-1α. *Exp Cell Res*. 2017;356:128–135.
57. Semenza GL. Vascular responses to hypoxia and ischemia. *Arterioscler Thromb Vasc Biol*. 2010;30:648–652.
58. Takeda Y, Costa S, Delamarre E, Roncal C, Leite de Oliveira R, Squadrito ML, Finisguerra V, Deschoemaeker S, Bruyere F, Wenes M, Hamm A, Serneels J, Magat J, Bhattacharyya T, Anisimov A, Jordan BF, Alitalo K, Maxwell P, Gallez B, Zhuang ZW, Saito Y, Simons M, De Palma M, Mazzone M. Macrophage skewing by Phd2 haplodeficiency prevents ischaemia by inducing arteriogenesis. *Nature*. 2011;479:122–126.
59. Lijkwan MA, Hellingman AA, Bos EJ, van der Bogt KEA, Huang M, Kooreman NG, de Vries MR, Peters HAB, Robbins RC, Hamming JF, Quax PHA, Wu JC. Short hairpin RNA gene silencing of prolyl hydroxylase-2 with a minicircle vector improves neovascularization of hindlimb ischemia. *Hum Gene Ther*. 2014;25:41–49.
60. Moraes F, Paye J, Mac Gabhann F, Zhuang ZW, Zhang J, Lanahan AA, Simons M. Endothelial cell-dependent regulation of arteriogenesis. *Circ Res*. 2013;113:1076–1086.
61. Shepherd AP, Öberg PÅ. *Laser-Doppler Blood Flowmetry*. Boston, MA: Kluwer Academic Publishers; 1990.
62. Yu AY, Shimoda LA, Iyer NV, Huso DL, Sun X, McWilliams R, Beaty T, Sham JSK, Wiener CM, Sylvester JT, Semenza GL. Impaired physiological responses to chronic hypoxia in mice partially deficient for hypoxia-inducible factor 1α. *J Clin Invest*. 1999;103:691–696.
63. Brusselmans K, Compernolle V, Tjwa M, Wiesener MS, Maxwell PH, Collen D, Carmeliet P. Heterozygous deficiency of hypoxia-inducible factor–2α protects mice against pulmonary hypertension and right ventricular dysfunction during prolonged hypoxia. *J Clin Invest*. 2003;111:1519–1527.
64. Owens GK, Kumar MS, Wamhoff BR. Molecular regulation of vascular smooth muscle cell differentiation in development and disease. *Physiol Rev*. 2004;84:767–801.
65. Pak O, Aldashev A, Welsh D, Peacock A. The effects of hypoxia on the cells of the pulmonary vasculature. *Eur Respir J*. 2007;30:364–372.
66. Schermuly RT, Dony E, Ghofrani HA, Pullamsetti S, Savai R, Roth M, Sydykov A, Lai YJ, Weissmann N, Seeger W, Grimminger F. Reversal of experimental pulmonary hypertension by PDGF inhibition. *J Clin Invest*. 2005;115:2811–2821.
67. Millette E, Rauch BH, Kenagy RD, Daum G, Clowes AW. Platelet-derived growth factor-BB transactivates the fibroblast growth factor receptor to induce proliferation in human smooth muscle cells. *Trends Cardiovasc Med*. 2006;16:25–28.
68. Imanishi M, Chiba Y, Tomita N, Matsunaga S, Nakagawa T, Ueno M, Yamamoto K, Tamaki T, Tomita S. Hypoxia-inducible factor-1α in smooth muscle cells protects against aortic aneurysms: brief report. *Arterioscler Thromb Vasc Biol*. 2016;36:2158–2162.
69. Yoshida S, Nabzdyk CS, Pradhan L, LoGerfo FW. Thrombospondin-2 gene silencing in human aortic smooth muscle cells improves cell attachment. *J Am Coll Surg*. 2011;213:668–676.
70. Grotendorst GR, Seppä HE, Kleinman HK, Martin GR. Attachment of smooth muscle cells to collagen and their migration toward platelet-derived growth factor. *Proc Natl Acad Sci U S A*. 1981;78:3669–3672.
71. Barnes EA, Chen C-H, Sedan O, Cornfield DN. Loss of smooth muscle cell hypoxia inducible factor-1α underlies increased vascular contractility in pulmonary hypertension. *FASEB J*. 2017;31:650–662.

SUPPLEMENTAL MATERIAL

Gene	Forward	Reverse
18s	5'-GAATTCCCAGTAAGTGCGGG-3'	5'-GGGCAGGGACTTAATCAACG-3'
Arnt	5'-GACAGACCACAGGACAGTTCC-3'	5'-AGCATGGACAGCATTTCTTGAA-3'
Fgf2	5'-ACCTTGCTATGAAGGAAGATGG-3'	5'-CAGTCGTTCAAAGAAGAAACACTC-3'
Glut1	5'-TCAACACGGCCTTCACTG-3'	5'-CACGATGCTCAGATAGGACATC-3'
Mmp3	5'-ACCAACCTATTCCTGGTTGCTGCT-3'	5'-ATGGAAACGGGACAAGTCTGTGGA-3'
Pai1	5'-AGGATCGAGGTAAACGAGAGC-3'	5'-GCGGGCTGAGATGACAAA-3'
Pdgfb	5'-CGGCCTGTGACTAGAAGTCC-3'	5'-GAGCTTGAGGCGTCTTGG-3'
Pdgfrb	5'-CTTCCACGAGGACGATGAGG-3'	5'-CTGCAGGTAGACCAGGTGAC-3'
Thbs1	5'-GCAGCACACACAGAAGCATT-3'	5'-CAATCAGCTCTCACCAGCAG-3'
Thbs2	5'-CACAGGTGGAGACAAGATGCT-3'	5'-TGAAGTGTCCTTGACGTGGT-3'
Timp1	5'-ACTCGGACCTGGTCATAAGGGC-3'	5'-TTCCGTGGCAGGCAAGCAAAGT-3'
Vegfa	5'-ACCAGACCTCTCACCGGAAA-3'	5'-GATGGCGTGGTGGTGACAT-3'

Table S1. qPCR primers

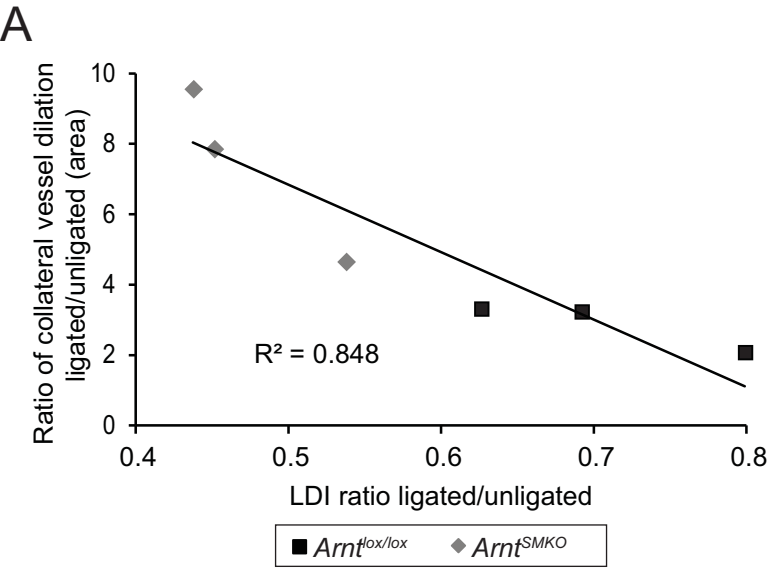

Figure S1. Collateral vessel lumen cross sectional area vs limb perfusion. (A) An inverse correlation is present between ratio of cross sectional area of collateral vessel lumens in ligated/unligated limbs and foot pad perfusion, reported as LDI ratio ligated/unligated; R^2=0.848; n=6.

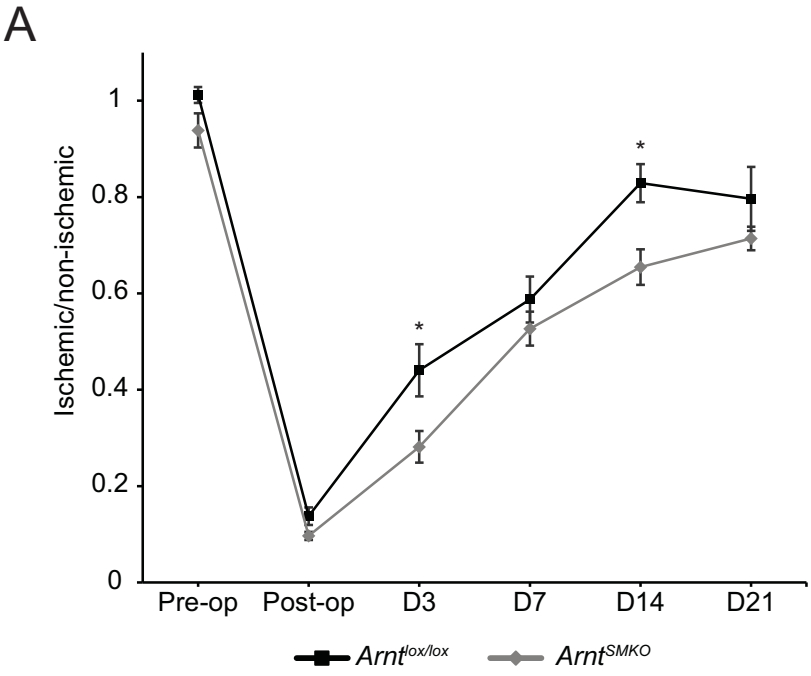

Figure S2. Proximal HLI model. The left femoral artery was ligated proximal to the deep femoral artery branch point in age- and gender- matched adult *Arnt*^{SMKO} and *Arnt*$^{lox/lox}$ mice. (A) Reduced perfusion, reported as a ratio of ligated/unligated limbs, was observed at days 3 and 14 in *Arnt*^{SMKO} mice; n=7, repeated-measures ANOVA: *p<0.05 *Arnt*^{SMKO} vs. *Arnt*$^{lox/lox}$.

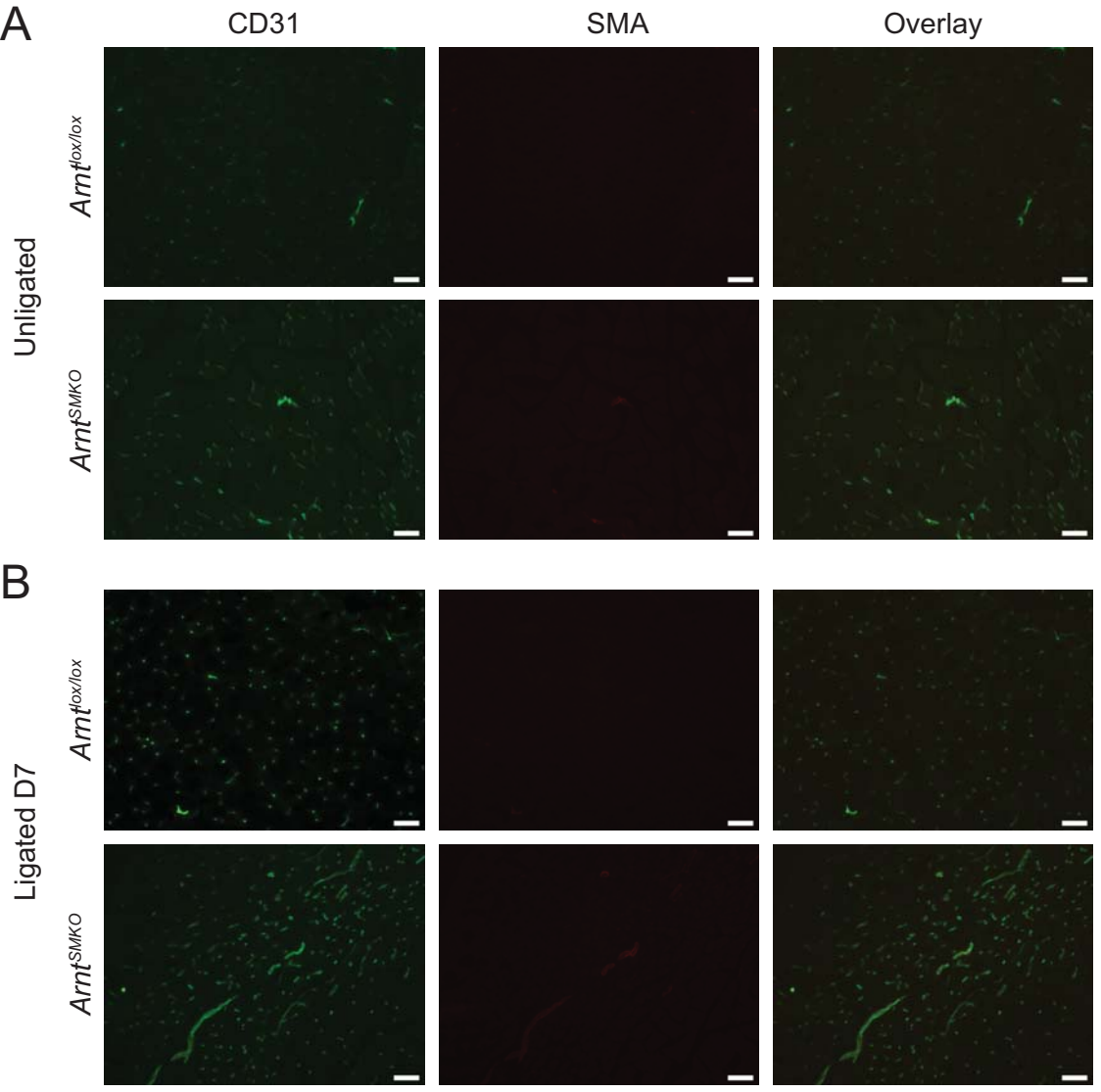

Figure S3. Capillary density and smooth muscle cell colocalization in gastrocnemius (GC) at day 7. Representative images of immunostained sections for CD31 labeled vessels (green) and α-smooth muscle actin (SMA, smooth muscle cells, red) from (A) unligated and (B) day 7 post ligation GCs. No apparent difference in number of SMA^{+} vessels between *Arnt*^{SMKO} and *Arnt*$^{lox/lox}$ in (A) unligated or (B) ligated day 7 limbs; n=3.

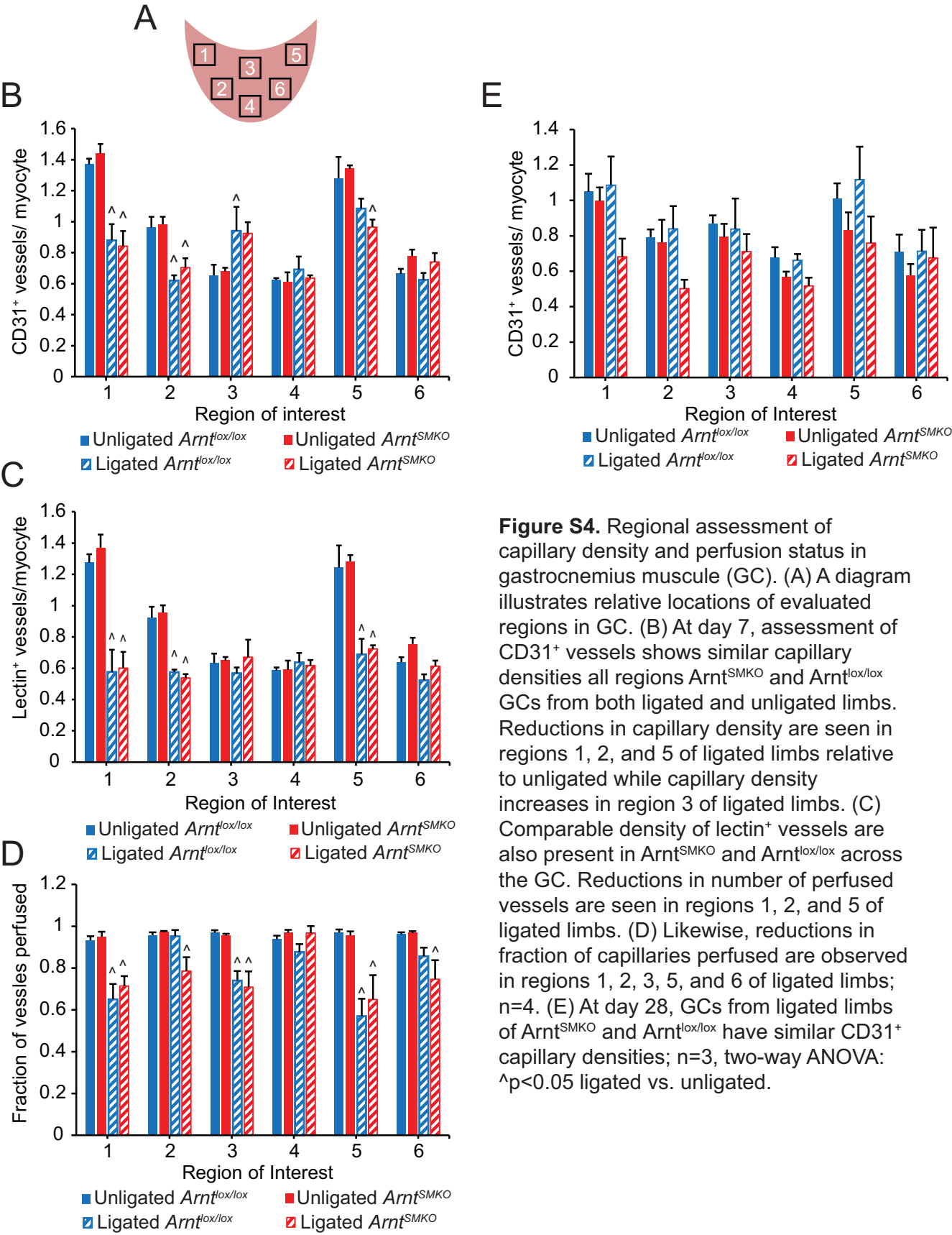

Figure S4. Regional assessment of capillary density and perfusion status in gastrocnemius muscule (GC). (A) A diagram illustrates relative locations of evaluated regions in GC. (B) At day 7, assessment of CD31⁺ vessels shows similar capillary densities all regions $Arnt^{SMKO}$ and $Arnt^{lox/lox}$ GCs from both ligated and unligated limbs. Reductions in capillary density are seen in regions 1, 2, and 5 of ligated limbs relative to unligated while capillary density increases in region 3 of ligated limbs. (C) Comparable density of lectin⁺ vessels are also present in $Arnt^{SMKO}$ and $Arnt^{lox/lox}$ across the GC. Reductions in number of perfused vessels are seen in regions 1, 2, and 5 of ligated limbs. (D) Likewise, reductions in fraction of capillaries perfused are observed in regions 1, 2, 3, 5, and 6 of ligated limbs; n=4. (E) At day 28, GCs from ligated limbs of $Arnt^{SMKO}$ and $Arnt^{lox/lox}$ have similar CD31⁺ capillary densities; n=3, two-way ANOVA: ^p<0.05 ligated vs. unligated.

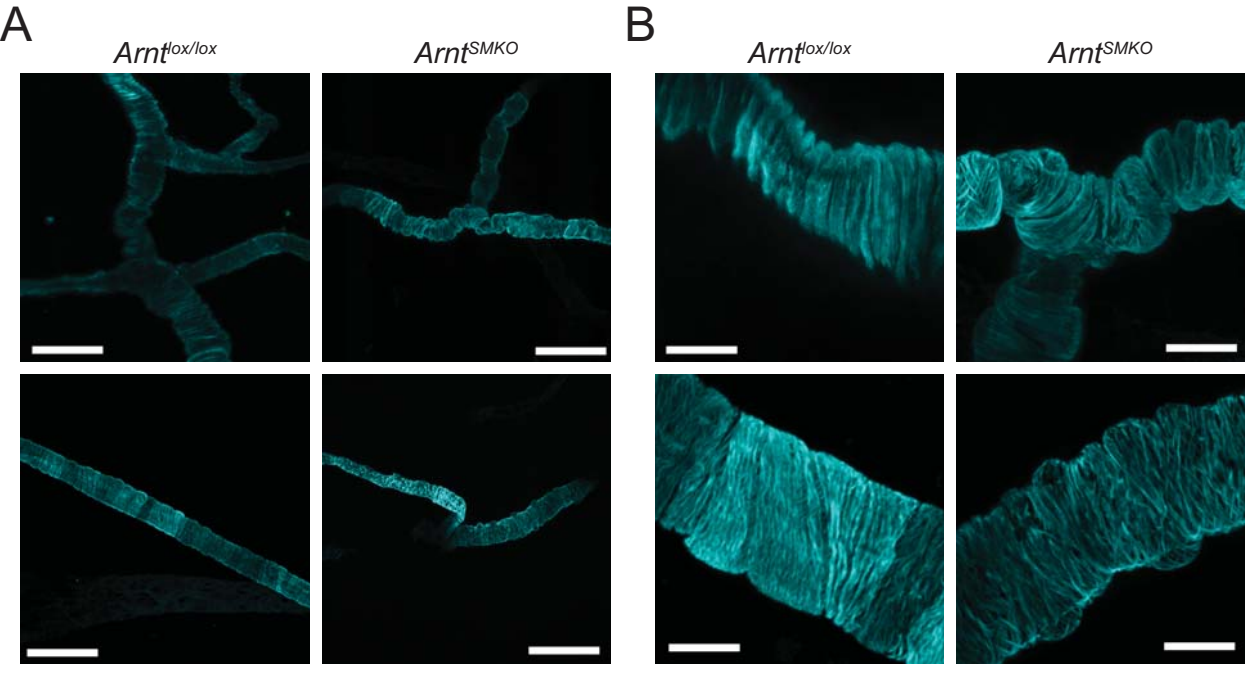

Figure S5. Additional images of arterioles in skeletal muscle. (A, B) Representative confocal images of SMA^+ VSMCs around small arterioles in spinotrapezius muscle illustrate disruption of organization and VSMC morphology in $Arnt^{SMKO}$. (A) Scale bars: 60μm. (B) Scale bars: 10μm.